Master's thesis

NTNU
Norwegian University of Science and Technology
Faculty of Economics and Management
Dept. of Industrial Economics and Technology Management

Tølløv Trønsdal Lyngstad

Flow-Based Market Coupling in Europe: Implications for the Nordic Power Market

Master's thesis in Industrial Economics and Technology Management
Supervisor: Asgeir Tomasgard
Co-supervisor: Paolo Pisciella and Stefan Jaehnert
June 2023

NTNU
Norwegian University of Science and Technology

Tølløv Trønsdal Lyngstad

Flow-Based Market Coupling in Europe: Implications for the Nordic Power Market

Master's thesis in Industrial Economics and Technology Management
Supervisor: Asgeir Tomasgard
Co-supervisor: Paolo Pisciella and Stefan Jaehnert
June 2023

Norwegian University of Science and Technology
Faculty of Economics and Management
Dept. of Industrial Economics and Technology Management

NTNU
Norwegian University of
Science and Technology

Preface

This thesis concludes my Master of Science in Industrial Economics and Technology Management at the Norwegian University of Science and Technology, Department of Industrial Economics and Technology Management.

I want to thank my supervisors, Professor and Director of FME NTRANS and The NTNU Energy Transition Initiative, Asgeir Tomasgard, and researcher at the Department of Industrial Economics and Technology Management, Paolo Pisciella, for their valuable input and helpful feedback.

I would also like to thank Sintef Energy Research for giving me the opportunity to write my thesis as a part of the research project "VannFly - The value of grid information in flow-based market coupling." A special thanks to Stefan Jaehnert, whose support and guidance have been paramount.

Trondheim, June 2023

Abstract

The power exchange Nord Pool paved the way for an increasingly interconnected European power market. Cross-border exchange capacity allows for better management of seasonal power supply and demand variations and accelerates the transition toward sustainable energy production. The rapid increase of renewable energy in Europe is expected to continue towards 2050, as coal and nuclear power are being phased out and replaced by variable renewable energy sources. These developments require more accurate exchange capacity calculation in the market clearing process.

Currently, the Nordic regions utilize the Coordinated Net Transfer Capacity methodology (CNTC) for capacity calculation. Under CNTC, electricity can be directly transferred between areas, constrained only by a pre-stated available transfer capacity. In contrast, Flow-Based Market Coupling (FBMC) considers the power grid's physical characteristics. FBMC is the preferred methodology by the European guidelines on capacity allocation and congestion management, and is set to be incorporated within the Nordic market in 2024, after multiple delays.

However, there is little published material regarding the implications of introducing FBMC in the Nordics; this highlights the need for further research and explains the delays in introducing the method in the Nordics. This report aims to address this by quantitatively analyzing the new methodology's effects on social welfare, power flows, and prices.

In the computational study, the implementation of FBMC substantially impacted power prices and flow patterns, allowing for easier identification of transmission lines with insufficient exchange capacity. Moreover, compared to the CNTC approach, it resulted in smaller price discrepancies between adjacent price areas. Additionally, the results pointed towards an increase in overall social welfare exceeding one million euros within a week, following the introduction of the flow-based methodology.

Sammendrag

Kraftbørsen Nord Pool ble oppretta i 1993 og la til rette for et stadig tettere integrert europeisk strømmarked. Utvekslingskapasitet på tvers av prisområder og landegrenser gjør det enklere å takle sesongvariasjoner i tilbud og etterspørel på en effektiv måte, og bidrar til å gjøre fornybar energiproduksjon mer lønnsomt og enklere å håndtere. EU og store deler av verden har forplikta seg til å nå netto null utslipp av klimagasser innen 2050, som betyr at kull og gass må erstattes av variable, fornybare energikilder som vind og sol i åra framover. Det vil føre til større prisvariasjoner, og det kreves derfor en mer presis kapasitetsberegning i markedsklareringa for å effektivt utnytte all tilgjengelig produksjonskapasitet.

I dagens markedsløsning oversetter Statnett som systemoperatør de faktiske nettkapasitetene til enkle handelskapasiteter mellom budområder, som deretter kommuniseres til markedet. Med flytbasert markedskobling (FBMC) blir i stedet de fysiske nettbegrensningene oppgitt direkte til markedet. Dette er en mer komplisert markedsløsning, som i teorien skal føre til en bedre utnyttelse av overføringskapasiteten i kraftsystemet. EUs retningslinjer peker på FBMC som den foretrukne markedsløsninga, og planen er å innføre flytbasert markedskobling i det nordiske markedet i løpet av 2024, etter gjentatte forsinkelser.

Det finnes imidlertid lite publisert materiale som omhandler konsekvensene av å innføre FBMC i de nordiske landene, og det er behov for mer forskning på området. I denne masteroppgaven ser jeg på hvordan innføringa av flytbasert markedskobling kan komme til å påvirke samfunnsøkonomi, kraftflyt og strømpriser.

Beregningsstudien viste at valg av markedsløsning har stor påvirkning på kraftflyten, og det ble enklere å identifisere overføringslinjer med utilstrekkelig utvekslingskapasitet med FBMC. Videre ble prisforskjellene mellom nabo-prisområder mindre med den flytbaserte markedsløsninga. Analysene indikerte dessuten at den samfunnsøkonomiske gevinsten av å innføre FBMC i Norden kan overstige én million euro i uka.

Contents

List of Figures

List of Tables

Terminology

AC	Alternating Current
ATC	Available Transfer Capacity
CACM	Capacity Allocation and Congestion Management
CNE	Critical Network Element
CNTC	Coordinated Net Transfer Capacity
CWE	Central Western Europe
DC	Direct Current
FanSi	Long-term power scheduling model developed by Sintef Energy Research
FBMC	Flow-Based Market Coupling
GSK	Generation Shift Key
MIP	Mixed Integer Programming
NP	Net Position
OPF	Optimal Power Flow
PriMod	Short-term power scheduling model developed by Sintef Energy Research
PTDF	Power Transfer Distribution Factor
RAM	Remaining Available Margin
RA	Remedial Action
TSO	Transmission System Operator
UCD	Unit Commitment and Dispatch

1 Introduction

The Nord Pool electricity market was the first transnational electricity market in the world and has provided the involved countries with stable market operation and well-functioning trading mechanisms for three decades. Cross-border transmission capacity ensures optimal production capacity utilization, allowing for better management of seasonal variations in supply and demand for energy and an accelerated transition toward sustainable energy production (Cui et al., 2021).

In the Nordic power market, power prices and exchanges are determined through the day-ahead market, wherein the transmission system operator (TSO) employs the Coordinated Net Transfer Capacity (CNTC) approach to translate physical limitations into bilateral transfer capacities between price zones, based on forecasts for the next day's supply and demand. However, this approach does not account for the physical attributes of a meshed power grid, as it does not consider the interdependencies of flows on interconnected transmission lines (Finck, 2021).

The increasing integration of renewable, intermittent energy sources in the energy mix has amplified the discrepancies between day-ahead commercial exchanges and realized physical flows. This trend is expected to continue until 2050, with the phaseout of coal and nuclear power due to environmental and safety concerns and the consequent replacement with variable renewable energy sources such as solar and wind power (Chen et al., 2021). In response to these developments, Flow-Based Market Coupling (FBMC) was introduced in the Central Western Europe region in 2015, aiming to provide more information about the physical grid topology directly to the market. The motivation is a more efficient and flexible use of the grid and higher socioeconomic welfare (Energinet et al., 2014).

The European Commission has established a guideline on capacity allocation and congestion management (CACM), wherein two permissible approaches for calculating cross-zonal capacity are identified: FBMC and CNTC. The flow-based approach is recommended as the primary approach for day-ahead and intraday capacity calculation. In contrast, the coordinated net transmission capacity approach is applicable only in regions where cross-zonal capacity is less interdependent, and the

TSO can prove that the flow-based approach does not bring added value (Commission Regulation (EU) 2015/1222, 2015).

FBMC is the preferred methodology by the CACM guidelines, and the Nordic TSOs are preparing for the introduction of FBMC as the capacity calculation method in the market. External parallel runs were published throughout 2022, and the target is to go live in the day-ahead market in 2024.

However, there is limited research investigating the specific impacts of introducing flow-based market coupling in the Nordics, and the need for further knowledge in this area is significant.

Outline

Chapter 2 explains the necessary background and theory to understand the importance of capacity calculation and the difference between the CNTC and the FBMC methodologies. Further, it contains an introduction to the market model PriMod, which is developed and used for the analysis in the thesis.

Chapter 3 provides an overview of relevant literature on capacity allocation and congestion management in Europe before the problem is formally described in Chapter 4. Next, Chapter 5 presents the model formulation, and Chapter 6 describes the input data and implementation. The empirical results are presented in the computational study in Chapter 7. Finally, Chapter 8 contains key takeaways from the analysis and discusses possible directions for future research.

2 Background

This chapter presents the necessary background and theory for this thesis. Section 2.1 describes the development of the Nordic power market and relevant power market mechanisms and terminology. Section 2.2 aims at providing the reader with an understanding of what FBMC is and how it compares to the current approach for capacity allocation and congestion management in the Nordics. Section 2.3 explains some fundamental relations in the field of power flow analysis, while 2.4 describes how the flow-based parameters are derived and computed. Some of the material in this chapter is inspired by the corresponding chapter in Lyngstad (2022).

2.1 The Nordic power market

The Nordic electricity industry underwent major transformations and deregulations during the 1990s, when a wholesale electricity market was established, exposing the energy suppliers to considerable competition. Nord Pool was formed in 1993 as a purely Norwegian power exchange before expanding to include Sweden in 1996, thereby becoming the world's first multinational power exchange (Flatabo et al., 2003). The Nordic market became fully integrated when Finland and Denmark joined in 1998 and 2000, respectively. Nord Pool paved the way for an increasingly interconnected European power market; in 2021, about 90 percent of the European power consumption was traded on the European day-ahead market (Olje- og energidepartementet, 2022).

The power market comprises a financial, physical, and consumer market, as summarized in Figure 2.1.

<table>
<tr><th>Financial Market</th><th colspan="3">Physical market</th><th>Consumer market</th></tr>
<tr><td rowspan="2">Nasdaq Inc.</td><td>Day-ahead</td><td>Intraday</td><td>Balancing</td><td rowspan="2">Producers and retailers</td></tr>
<tr><td colspan="2">Nord Pool</td><td>Statnett</td></tr>
</table>

Figure 2.1: The Nordic power market elements and the organizers in the Norwegian power system.

The consumer market participants range from private households purchasing electricity from retail providers to power-intensive firms buying directly from the physical market. The financial market provides derivatives for risk management, hedging, or speculation by participants without physical deliveries. Finally, the physical market, where the CACM methodology impacts the market clearing process, includes the day-ahead, intraday, and balancing markets.

The **day-ahead market** is for hourly power exchanges for the next 24 hours. The Nord Pool markets are divided into bidding zones, or price areas, determined by the TSO. Market participants submit their offers before the auction closes at 12:00 PM, after which Nord Pool establishes an equilibrium between aggregated supply and demand curves for all price areas. With unlimited transmission capacity, this price formation scheme would ensure optimal allocation of the available production capacity and an equal power price for the market. However, transmission capacity is not unlimited, thus necessitating a capacity calculation methodology. Figure 2.2 illustrates the daily routines in the day-ahead price formation scheme.

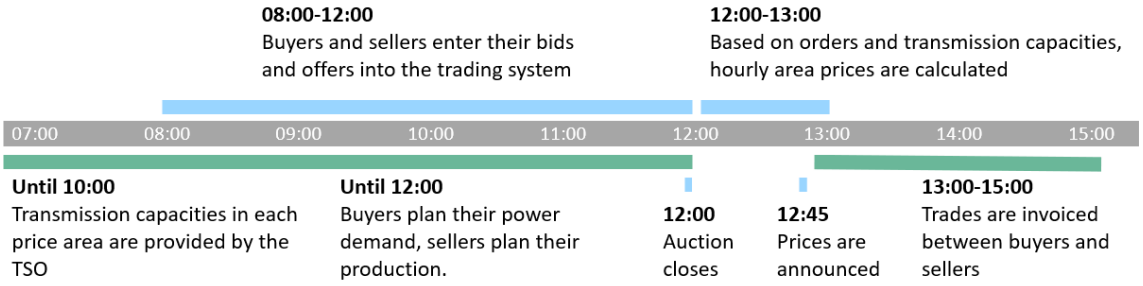

Figure 2.2: Timeline illustrating the daily routines in the day-ahead market, as run by Nord Pool (Sutter, 2014).

Bottlenecks in the transmission system are reflected in differing area prices across neighboring bidding zones. In such cases, the TSO collects a *congestion rent*, calculated as the product of the exchanged power and the price difference (Farahmand, 2021). High congestion rents indicate a constrained grid infrastructure, and the extra income for the TSO is earmarked for infrastructure development and maintenance. The calculation of the congestion rent is illustrated in Figure 2.3 below.

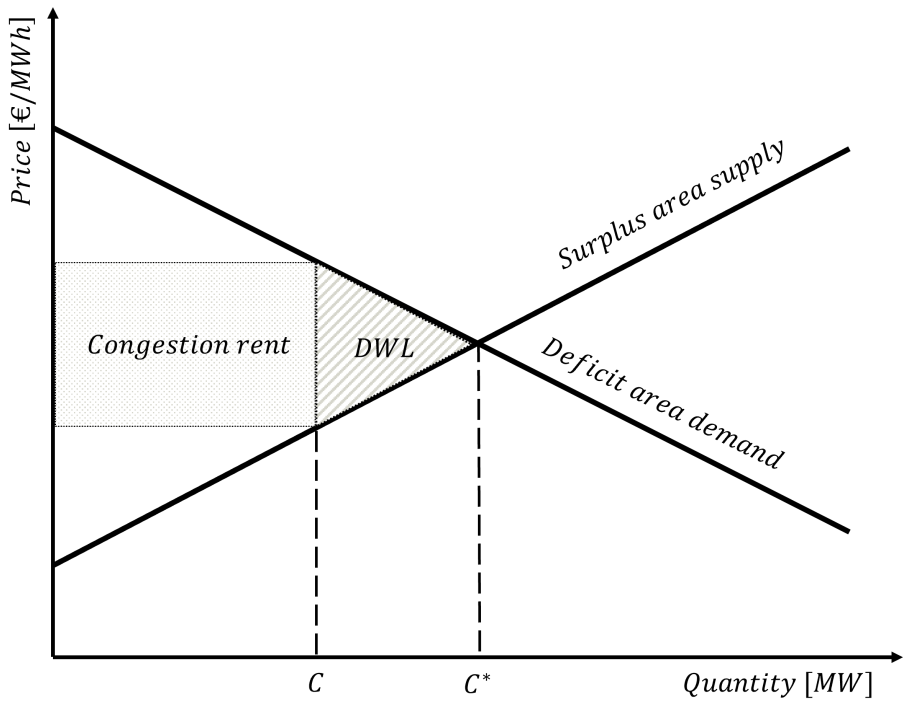

Figure 2.3: Congestion rent and deadweight loss due to limited capacity between two areas. C is the actual capacity, C^* is the required capacity for full price convergence.

With the current CNTC approach, the TSO publishes the available transfer capacities (ATCs) between bidding zones during the auction based on forecasts for tomorrow's operating conditions. After receiving offers and assessing available transfer capacity, the market is settled, and power prices for the next day are announced at 12:45 PM.

The increasing share of variable renewable energy sources in the market complicates the market participants' balance after the day-ahead market's closure (Nordpoolgroup, 2020). Therefore, the **intraday market** offers the opportunity to trade and ensure balance until one hour before the operating hour to address these deviations between the day-ahead offers and realized production or demand.

The **balancing market**, operated by the TSO, regulates the power balance during operation. The TSO ensures the availability of sufficient balance reserves and takes corrective actions when needed to ensure stable operation.

2.2 FBMC in brief: Concepts and methodology

Market coupling, or the interconnection of independent supply and demand areas, allows for cross-regional and cross-border import and export. In 2014, the European Union launched *Euphemia*, a price coupling algorithm that marked a significant market coupling project encompassing many of Europe's largest power exchanges (Bjorndal et al., 2018b). A critical challenge in integrating these markets is efficiently managing cross-border network congestion.

As the power market becomes increasingly interconnected, the benefits of a precise capacity calculation methodology become more significant. The capacity calculation aims to convert physical transmission limits in the power grid to commercial exchange capacities in line with operational security and market design requirements. Under the CNTC methodology, the TSO provides market participants with limits on the allowable exchange between adjacent price areas. These limits, determined by the physical capacity minus a security margin, do not consider the interconnected network's cross-border flow interdependencies, leading to large security margins and potential discrepancies between commercial and physical flows (Bjorndal et al., 2018a).

In contrast, FBMC limits the net export of all bidding zones simultaneously, capturing power flow interdependencies for the entire coupled market more comprehensively. Consequently, more of the physical capacity can be made available to the market (Weinhold and Mieth, 2022). The capacity allocation is not made by the TSO but driven by the market at the time of allocation, allowing for more efficient use of the power grid. FBMC provides more trading opportunities while maintaining the same security level, reducing price differences across exchange borders, and enhancing social welfare (Weinhold, 2021). It also brings the commercial flow closer to the physical realization of the power flow.

Alternatively, a nodal pricing scheme could be introduced, in contrast to the current zonal scheme in Europe with uniform prices within bidding zones. Though successfully implemented in several regions, nodal pricing is no longer under consideration for the European market (Bjorndal et al., 2018a). FBMC is the preferred option in the

EU CACM guidelines and will be introduced in the Nordics in 2023. The generic market optimization problem is formulated below, where NP_a (net position) is the net injected power to the grid from area a.

CNTC	FBMC
max social welfare	max social welfare
$NP_a = Supply_a$ - $Demand_a$, $a \in \mathcal{A}$	$NP_a = Supply_a$ - $Demand_a$, $a \in \mathcal{A}$
$\sum_a NP_a = 0$	$\sum_a NP_a = 0$
CNTC constraints	FBMC constraints

The objectives are the same, but the binding constraints differ. The feasible region using the FBMC approach will generally be larger than or equal to that of the CNTC approach. Still, as demonstrated by Van den Bergh et al. (2016), the CNTC domain can be structurally different from the flow-based domain and even include some solutions that are not part of the flow-based domain.

2.2.1 Three-node example

To illustrate the differences between the two methodologies, consider a classical three-node sample system, illustrated in Figure 2.4 below.

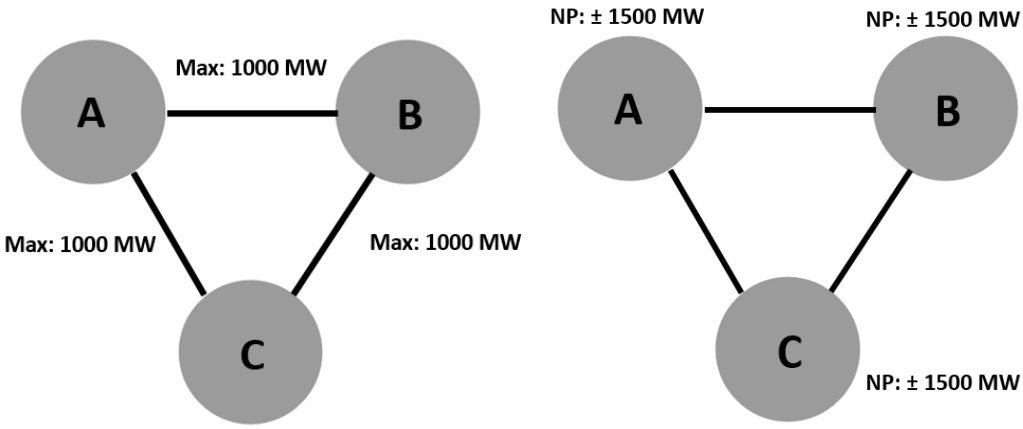

(a) Transmission capacity

(b) Max import/export of each node using CNTC

Figure 2.4: A simple three-node power system.

Each transmission line in this system has equal impedances and transmission capacities of 1000 MW. The net positions' maximum and minimum values in Figure 2.4 (b) result from the grid properties. Power transfer distribution factors (PTDFs) describe these properties. A PTDF is a sensitivity factor describing how a change in the net position at a node affects the power flow on the system's transmission lines. PTDFs can be calculated based on the line impedances and a selected slack node (this is detailed in Section 2.4). If node C is the slack node, the system's PTDFs are as presented in Table 2.1.

Table 2.1: PTDFs of the three-node sample system

Line	Node A	Node B	Node C
AB	0.33	-0.33	0
AC	0.67	0.33	0
BC	0.33	0.67	0

Each line's PTDF values are identical but inverted for the opposite flow direction (i.e., BA, CA, and CB). In the CNTC methodology, PTDFs are not provided to the market algorithm. Instead, available transfer capacities are given to the market without any information about the grid's physics. The market thus perceives the capacities as simultaneously available, and the total capacity of the grid cannot be fully utilized because power flows equal to the ATCs on all transmission lines must be feasible at the same time.

The PTDF of line AC indicates that the net position at node A will induce a flow of $NP_a \cdot 0.67$ on line AC. A net position at node A above 1500 MW will generate a flow on AC that breaches the 1000 MW capacity constraint, which explains the net position limits from Figure 2.4 (b). Note how a negative net position at node B could counterbalance the overload, but this information is not available to the market clearing algorithm in the CNTC methodology. Instead, the TSO must limit the total export from node A to 1500 MW by, for example, setting an available transfer capacity of 750 MW on both line AC and AB to avoid overloads. The same logic applies to all three nodes. The feasible region of the CNTC approach is illustrated in Figure 2.5 below, in black font.

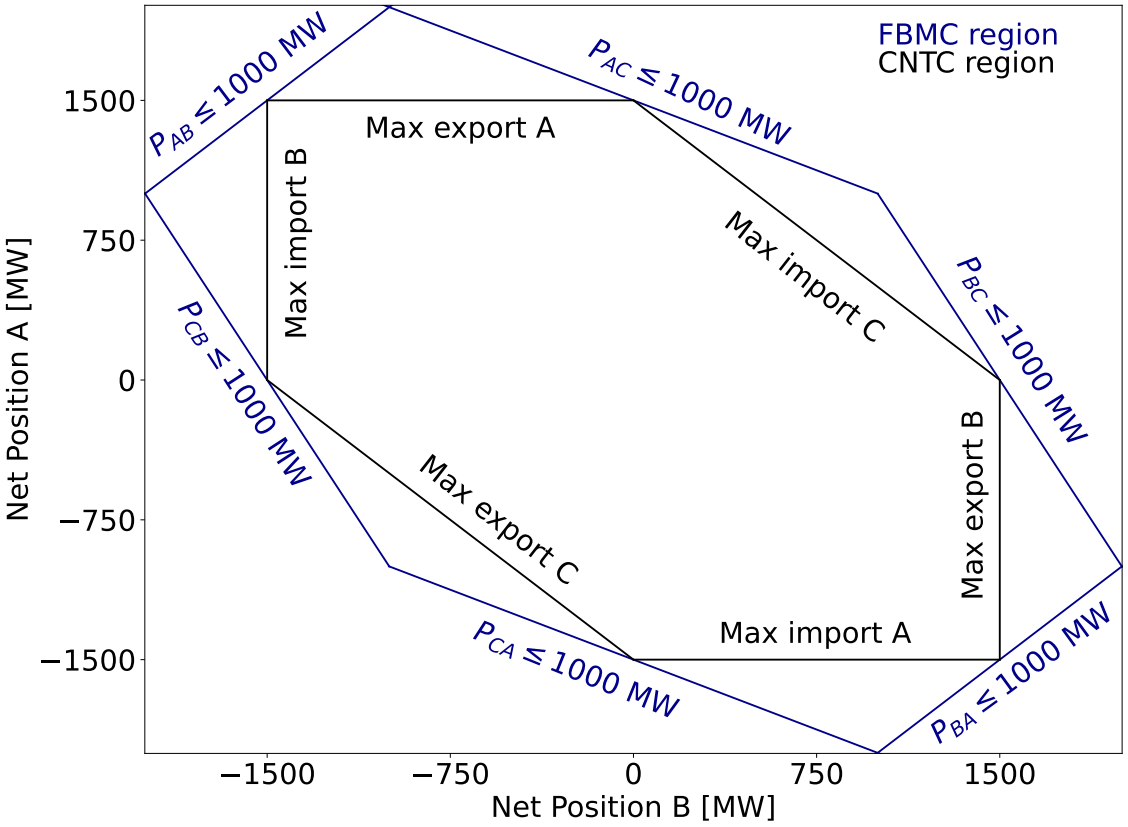

Figure 2.5: Feasible region using CNTC and FBMC on the sample system.

Note that an ATC value of 750 MW on all lines is one of several possible ATC configurations. The key takeaway is that the TSO must limit the power flows to ensure that overload does not happen. With FBMC, on the other hand, the PTDFs describing the system are made available to the market. The entire system and the nodes' interactions are considered when determining possible market solutions, aligning the market clearing more closely with the grid's physical properties. This allows for new solutions previously unavailable with CNTC, because any market clearing under the FBMC approach will be physically feasible, and the TSO will no longer have to limit the transmission capacity to below 1000 MW. The flow P_{ij} on each line is determined by the net positions and the PTDFs from Table 2.1:

$P_{AB} = 0.33NP_A$ - 0.33 NP_B	$P_{BA} =$ -0.33NP_A + 0.33 NP_B
$P_{AC} = 0.67NP_A$ +0.33 NP_B	$P_{AC} =$ -0.67NP_A - 0.33 NP_B
$P_{BC} = 0.33NP_A$ + 0.67 NP_B	$P_{BC} =$ -0.33NP_A - 0.67 NP_B

One new, feasible solution is NP_A = 2000 MW, NP_B = -1000 MW, and NP_C = -1000 MW, inducing a flow of 1000 MW on AC and AB, and 0 MW on BC. Figure 2.5 illustrates the feasible region constituted by the six power flow equations above being restricted to 1000 MW in blue font.

Power flows of 1000 MW are now feasible because the market clearing will never allow it to happen simultaneously at all three lines. On the other hand, using the CNTC methodology and setting the ATCs = 1000 MW on all three connections, a solution with $P_{AC} = P_{BC} = P_{AB} = 1000$ MW is a feasible market solution but an infeasible physical solution. Thus, the ATC values must be limited to ensure that power flows equal to the ATC on all three lines are simultaneously feasible, which is why the FBMC approach offers a larger feasible region.

2.3 Power flow analysis

Power flow analysis is the study of a power system's steady-state operation. It is an essential part of the TSOs' task of controlling the system, providing the operator with information about congested network elements and nodal voltages. A brief introduction to power flow analyses is necessary to understand how the grid information in the flow-based methodology is derived.

2.3.1 AC power flow

In a system of n nodes, the net injected currents at each node can be expressed as a function of branch admittances and nodal voltages. On matrix form , we have:

$$\left[I \right] = \left[Y \right] \left[V \right]$$

The Y matrix, known as the nodal admittance matrix, holds information about the network topology. Each admittance y_{ij} on a line consists of the conductance g_{ij} and susceptance b_{ij}. The conductance $g_{ij} = 1/r_{ij}$ is the inverse of the line resistance, and the susceptance $b_{ij} = 1/x_{ij}$ is the inverse of the line reactance. The diagonal terms of the Y matrix contain the sum of all branch admittances y_{in} for all nodes n connected directly to the corresponding node i. The off-diagonal elements contain

the negative of the branch admittance y_{ij} connecting the nodes i and j.

The net injected complex power S at node i can be expressed using polar notation:

$$S_i = V_i I_i^* = V_i \big[\sum_{j=1}^{n} Y_{ij} V_i \big]^* \tag{2.1}$$

$V_i = |V_i| e^{j\delta_i}$ is the complex node voltage at node i, and $Y_{ij} = G_{ij} + jB_{ij} = |Y_{ij}| e^{j\theta_{ij}}$ is element ij of the nodal admittance matrix. We obtain the injected real and reactive power P_i and Q_i by applying Euler's formula and resolving Equation 2.1 into real and imaginary parts.

$$P_i = |V_i| \sum_{j=1}^{n} |V_j||Y_{ij}| \cos(\delta_i - \delta_j - \theta_{ij}) \tag{2.2}$$

$$Q_i = |V_i| \sum_{j=1}^{n} |V_j||Y_{ij}| \sin(\delta_i - \delta_j - \theta_{ij}) \tag{2.3}$$

The power flow on a line between two connected nodes i and j is determined by the branch admittance and the node voltages with the following relation:

$$S_{ij} = V_i I_{ij}^* = V_i \big[\big(V_i - V_j\big) y_{ij} \big]^* \tag{2.4}$$

2.3.2 DC power flow

Equations 2.2 and 2.3, commonly referred to as the *power flow equations*, are non-linear and pose challenges in solving, especially when analyzing large networks. A frequently used alternative in such situations is the DC power flow analysis, a linear approximation of the power flow equations (Frank and Rebennack, 2016). The following assumptions are made:

- Line reactances are much larger than line resistances:
  $x_{ij} >> r_{ij} \implies y_{ij} = g_{ij} + jb_{ij} \approx jb_{ij} \implies Y_{ij} \approx |Y_{ij}| e^{j90^\circ} \implies \theta_{ij} = 90^\circ$
- Node voltage magnitudes are close to rated values:
  $|V_i| \approx |V_{nom}| \implies |V_i| = 1\ [p.u]$.
- Node voltage angle differences are minor: $\delta_i \approx \delta_j$

Given these assumptions and recognizing that for small values of x, sine and cosine can be approximated to $sin(x) \approx x$ and $cos(x) \approx 1$, we can simplify the power flow equations to obtain Equations 2.5 and 2.6. These represent the real and reactive power injection at node i in the network:

$$P_i = \sum_{j=1}^{n} |Y_{ij}|(\delta_i - \delta_j) \tag{2.5}$$

$$Q_i = -\sum_{j=1}^{n} |Y_{ij}| \tag{2.6}$$

Only the magnitudes of the Y matrix elements remain in the DC power flow equations. Reactive power flow becomes a constant term proportional to the network admittances and does not impact the system (Energinet et al., 2014). Therefore, DC power flow studies do not consider reactive power flow. Equation 2.5 can be expressed in matrix form as:

$$\left[P \right] = \left[Y_{DC} \right] \left[\delta \right] \tag{2.7}$$

Here, Y_{DC} is equivalent to the node admittance matrix but with only the magnitudes of the elements retained. Equation 2.7 has an infinite set of solutions, as the injected power depends on the voltage angle differences, not their absolute values. To obtain a unique solution, a node is chosen as the *slack node* ($\delta_{slack} = 0$), providing a reference point in the system. If node i is the slack node, row and column i from the Y_{DC} matrix are eliminated, allowing a unique solution to be calculated.

Under these assumptions, the power flow on a line simplifies to:

$$P_{ij} = |Y_{ij}|(\delta_i - \delta_j) \tag{2.8}$$

Due to its computational efficiency compared to more complex and non-linear AC power flow models, DC power flow is commonly used in large-scale power system analysis, optimization, and planning studies. It provides a reasonable approximation for systems where the effects of reactive power and line losses are minor compared to the active power flow.

2.3.3 DC optimal power flow

Optimal power flow (OPF) is a mathematical optimization problem widely used in power systems engineering to determine the optimal power generation dispatch in an electric power network while considering various operational constraints. The objective of an OPF model is typically to minimize the overall generation cost, maximize system efficiency, or achieve other specific goals, such as voltage stability or renewable integration.

A simplified version of this, known as DC optimal power flow (DC-OPF), approximates the AC power flow model with a linear DC power flow model, as discussed in the previous section. Below is a compact formulation of the DC-OPF problem (Frank and Rebennack, 2016).

$$\min \quad \sum c^T p \tag{2.9}$$

$$\text{s.t.} \quad p = Y_{DC}\,\delta \tag{2.10}$$

$$P_{min} \leq p \leq P_{max} \tag{2.11}$$

The objective function minimizes total generation cost. Constraint 2.10 is the set of DC power flow equations, while (2.11) restricts power outputs to their operating range. Although more comprehensive OPF formulations also consider branch current limits (i.e., restricting the line flows defined in Equation 2.8 to defined transmission capacities), these have been omitted in the formulation above for simplicity.

DC-OPF is used for large-scale power system optimization and planning studies where computational efficiency is important. Despite its simplifications, DC-OPF remains a valuable tool in power systems engineering due to its computational efficiency and versatility in various applications.

2.4 FBMC parameters

The primary advantage of the FBMC methodology over the CNTC approach is that the physical properties of the grid are represented in the market clearing algorithm. This grid information is made available to the market through power transfer distribution factors and remaining available margins. This section will describe these parameters and how they are established.

2.4.1 Power transfer distribution factors

The fundamental input parameters in the FBMC methodology are the PTDFs, which express how a change in net position in one price area influences the power flow in the system. These factors are calculated based on a DC power flow approximation of the system.

Consider the Y_{DC} matrix established in Section 2.3.2. Instead of eliminating the row and column corresponding to the chosen slack node i, an alternative approach to finding a unique solution is to add +1 at position ii in the matrix. The voltage angles at every node, including the slack node, will then vary with changes in the power injections according to the relation below:

$$\left[\,\Delta\delta\,\right] = \left[\,Y_{DC}\,\right]^{-1}\left[\,\Delta P\,\right]$$

The inverted Y_{DC} matrix is often referred to as the Z_{DC} matrix. The change in voltage angle at node i caused by a net injection change at node n can be expressed as:

$$\Delta\delta_i = \Delta P_n(Z_{DC,\,in}) \tag{2.12}$$

Recalling the line flow defined in Equation 2.8, the line flow *change* caused by a net injection change at node n can be described by:

$$\Delta P_{ij} = |Y_{ij}|(\Delta\delta_i - \Delta\delta_j) = |Y_{ij}|\Delta P_n(Z_{DC,\,in} - Z_{DC,\,jn}) \tag{2.13}$$

Note that the net injection P_n at node n is equivalent to the net position at the node.

Finally, the definition of the PTDF of node n on line ij is established:

$$ptdf_{ij}^{n} = \frac{\Delta P_{ij}}{\Delta P_{n}} = |Y_{ij}|(Z_{DC,\,in} - Z_{DC,\,jn}) \tag{2.14}$$

In a nodal pricing scheme, the PTDFs are calculated for all nodes and connections in the power system and applied in the market algorithm. In the FBMC methodology, the PTDFs are instead aggregated to price areas and critical network elements (CNEs). Critical network elements are power system components vulnerable to overloads, such as transmission lines between price areas, transformers, or cross-border DC cables. A network element is considered critical if the TSO assesses its power flow to be heavily influenced by the cross-zonal exchange. This selection process prevents transmission lines insensitive to net position changes from limiting cross-zonal exchange capacities (Weinhold and Mieth, 2022).

The aggregation process is not trivial because any node within a price area uniquely influences every CNE in the network. The FBMC methodology uses generation shift keys (GSK) to describe how the net position of a single node impacts the net position in the price area. Numerous GSK strategies exist, and Statnett is still conducting analyses to determine how to make the aggregation process sufficiently accurate (Hirvonen, 2022).

The GSK value translates the PTDFs of all nodes n in the price area to a single PTDF for area a. The following two equations formally express the relationship between nodal and zonal PTDFs:

$$ptdf_{ij}^{a} = \sum_{n \in a} gsk^{n} \cdot ptdf_{ij}^{n}, \qquad \sum_{n \in a} gsk^{n} = 1 \tag{2.15}$$

The most straightforward GSK strategy is a flat participation scheme where each node within an area is assigned equal weight. While uniform GSKs are less accurate than more sophisticated strategies, such as those proportional to nodal power production or net injection, the latter require a precise forecasting methodology (Energinet et al., 2014).

2.4.2 Remaining available margins

The other fundamental input parameters in the FBMC methodology are the remaining available margins (RAM) on the critical network elements. They correspond to the available transfer capacities in the CNTC approach but are generally larger. For instance, in the three-node example from Section 2.2, the RAM on each line equals the total transmission capacity of 1000 MW, whereas the ATC is limited to 750 MW. In practice, the RAM value is set smaller than the transmission line capacity to compensate for uncertainties and errors associated with the PTDF calculations. The RAM on a transmission line ij is defined in Equation 2.16.

$$RAM_{ij} = F_{ij}^{max} - FRM_{ij} - F_{ij}^{ref'} \tag{2.16}$$

F_{ij}^{max} is the maximum line capacity, while FRM_{ij} is the Flow Reliability Margin, which acts as an operational security margin. The magnitudes of the FRMs are determined through a statistical evaluation of deviations between the day-ahead FBMC market flows and the actual physical flows. To foster competition and better integration of renewable energy sources, EU regulations stipulate that at least 70% of the thermal capacity must be made available to the market, i.e., the FRMs are kept below 30% (Regulation (EU) 2019/943, 2019). The final term, $F_{ij}^{ref'}$, is defined in Equation 2.17.

$$F_{ij}^{ref'} = \underbrace{\sum_{n} ptdf_{ij}^{n} \cdot NP_n}_{physical\ flow\ F_{ij}^{ref}} - \underbrace{\sum_{a} ptdf_{ij}^{a} \cdot NP_a}_{market\ flow} \tag{2.17}$$

Note the distinction between $F_{ij}^{ref'}$ and F_{ij}^{ref}, a notation established by Energinet et al. (2014), and illustrated in Figure 2.6 below. The market flow from Equation 2.17 is the flow on the transmission line in a market solution to the forecasted state of the system. Thus, it is calculated using zonal net positions and PTDFs, which are aggregated with an appropriate set of GSKs. On the other hand, the physical flow F_{ij}^{ref} is calculated with nodal net positions and PTDFs. $F_{ij}^{ref'}$ accounts for the discrepancy between the market flow and the physical, DC-approximated flow. It is subtracted from the thermal capacity, F_{ij}^{max}, to account for errors related to

the aggregation from nodal to zonal PTDFs. For a more detailed explanation of the RAM value calculation, see Energinet et al. (2014). The parameters and their relations are illustrated in Figure 2.6 below.

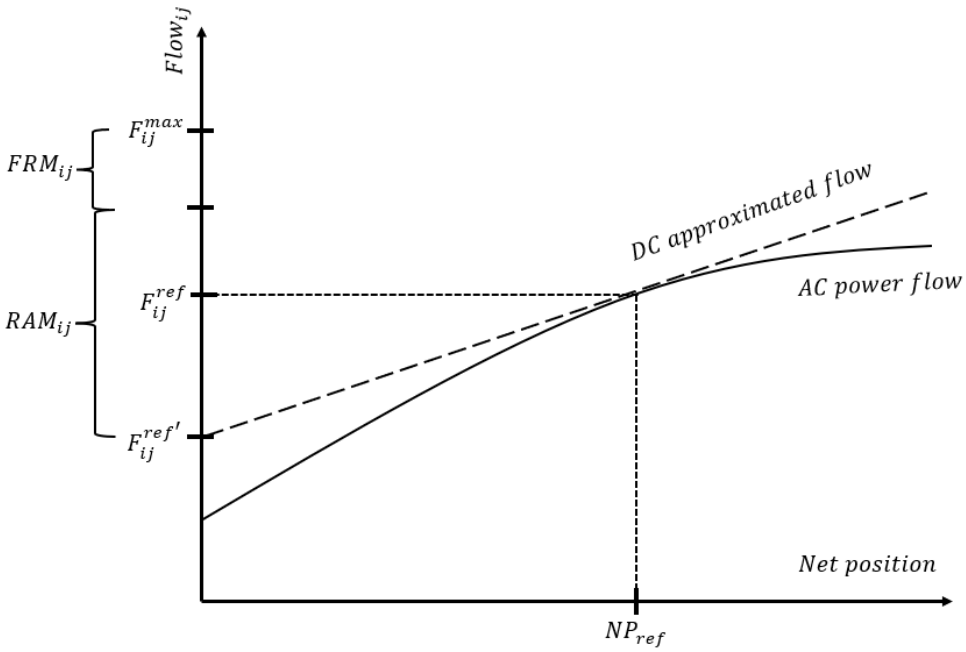

Figure 2.6: RAM calculation parameters (Energinet et al., 2014).

The more accurate representation of the grid's physical properties in the FBMC methodology allows for a less conservative estimation of the RAM parameters compared to the corresponding ATC values in the CNTC approach. This is why the flow-based domain is typically larger than the CNTC domain (Van den Bergh et al., 2016). The primary sources of uncertainty are related to the DC approximation of the power system and the precision of the GSK strategy in translating nodal power injections to zonal injections (Energinet et al., 2014).

In summary, the grid constraints distinguish the CNTC from the FBMC methodology. These constraints can be generically formulated as follows:

CNTC	FBMC
$flow_{ij} \leq ATC_{ij}$	$\sum_a ptdf_{ij}^a \cdot NP_a \leq RAM_{ij}$

2.5 PriMod: A short-term power market model

Sintef Energy Research developed the hydrothermal scheduling model, PriMod, as part of the project "Pricing Balancing Services in the Future Nordic Power Market" (PRIBAS). PriMod is a short-term mixed-integer programming (MIP) model written in Python using the open-source optimization modeling language Pyomo. Part of a larger scheduling toolchain, PriMod is designed to tackle unit commitment and least cost dispatch problems over a short time horizon in hydro-dominated power systems, provided exogenously given long-term water values. It was developed to meet the rising demand for flexibility and control in light of the increasing share of intermittent renewable power. It aims to provide accurate information for investment decisions in increasingly complex systems, which require greater detail in describing the physical system and representing uncertainty than previous market models offer (Haugen and Helseth, 2021).

Operational power planning in hydro-thermal systems can be categorized into long-term, seasonal, and short-term scheduling. Previously, Nordic operational planning relied solely on long-term models. While models like FanSi cover lengthy time horizons and multi-dimensional stochastic processes, they compromise on time resolution and technical detail. PriMod, however, allows for time resolutions down to 15 minutes.

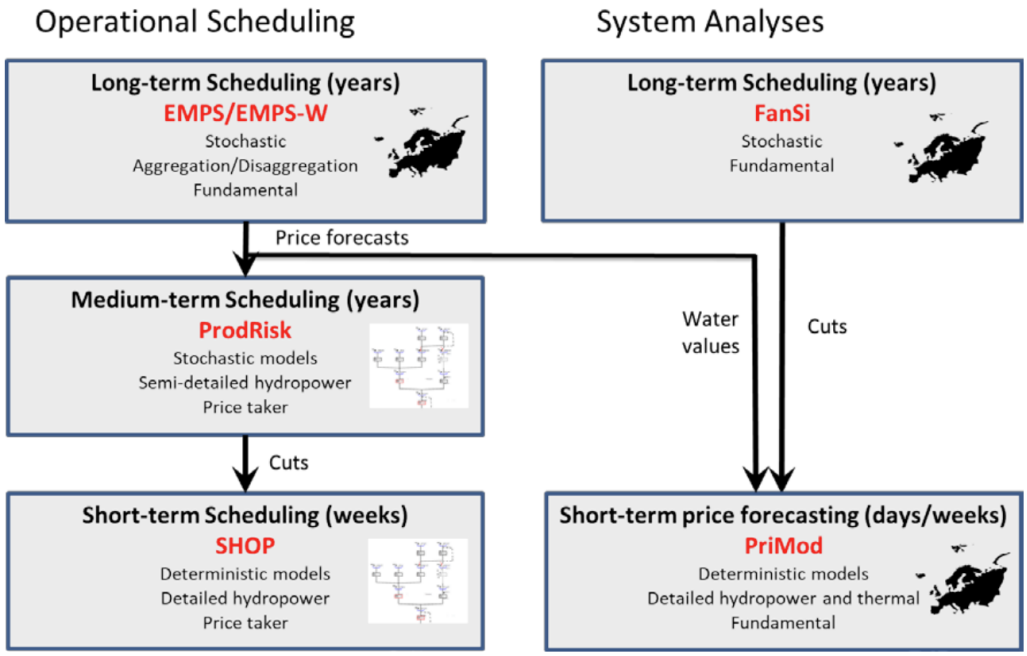

Figure 2.7: Sintef's scheduling toolchain (Haugen and Helseth, 2021).

Figure 2.7 illustrates Sintef's scheduling toolchain, used by numerous market participants in the Nordic power market. The strategic model FanSi solves the long-term hydro-thermal scheduling problem. It decides weekly actions by solving a two-stage stochastic linear programming problem, with uncertainty in weather conditions represented by a fan of scenarios (Helseth et al., 2018). Figure 2.8 below illustrates how water values from the long-term model FanSi are received as input parameters in PriMod, in the form of Bender's cuts for each week. These cuts indicate the expected future cost of operating hydropower from the upcoming week as a function of the hydro reservoir levels at the end of the current week.

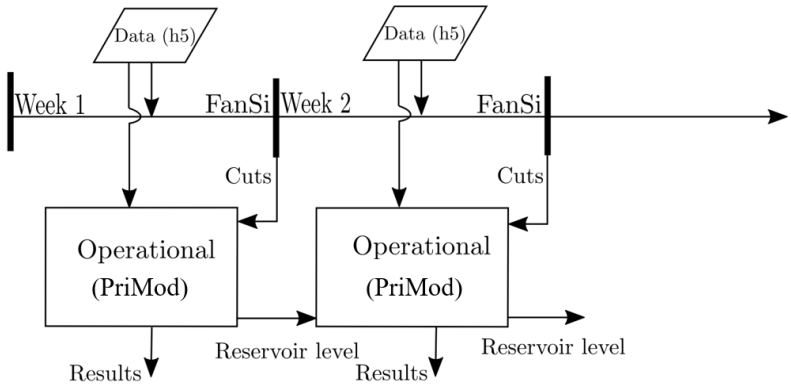

Figure 2.8: Coupling between FanSi and PriMod (Helseth et al., 2018).

PriMod was developed to re-optimize the weekly decision problem with a finer time resolution and more detailed modeling than provided with FanSi.

PriMod has two stages: the unit commitment and dispatch (UCD) stage and the balancing stage. These stages reflect the different stages of the power market detailed in Section 2.1. In essence, PriMod solves the daily UCD problem, provided an end-of-horizon valuation of stored water from FanSi. The model is solved using a rolling 48-hour horizon. After resolving the 48-hour UCD problem, the solution is forwarded to the balancing problem before the model proceeds to the next step. The balancing stage is optional and will not be included in the analyses in this thesis, to reduce complexity.

3 Literature review

FBMC was introduced in the Central Western Europe (CWE) area in 2015. Numerous studies have assessed the effects on prices, power flows, and social welfare before and after it was introduced. However, few published articles examine the introduction of FBMC in the Nordic market. This section will provide an overview of the available literature on FBMC in the Nordics, supplemented by key findings from the extensive literature on FBMC in CWE. Parts of this chapter are based on the corresponding chapter in Lyngstad (2022).

3.1 Literature search strategy

To identify papers on FBMC and its impacts on the Nordic power system, a systematic literature search was conducted using Google Scholar. The search focused on the terminology established in the classical paper by Schavemaker and Beune (2013). Insights on how FBMC compares to the CNTC methodology and to a nodal pricing scheme as an optimal benchmark were prioritized. Table 3.1 provides an overview of the key terms utilized in the search. After the initial search, numerous articles were identified and filtered based on relevance in titles and abstracts. The most relevant papers were selected and included in the subsequent sections of this study.

Table 3.1: Literature search: overview and selected keywords.

Pricing scheme	CACM Approach	Keywords
Zonal	CNTC	Social welfare, price convergence, total exchange, re-dispatch, congestion management
	FBMC	
Nodal	Nodal pricing	

3.2 Capacity allocation and congestion management

The primary motivation for introducing FBMC is the increased social welfare due to better utilization of the available grid capacity. Consequently, examining the difference between CNTC and FBMC in terms of social welfare is a key objective in most studies on FBMC. Bø et al. (2020) studied three supply and demand scenarios for the Nordic power market. They compared CNTC to FBMC in each scenario, using a one-year deterministic cost minimization model with static grid restrictions throughout the year. They found significant social welfare increases with FBMC in all three scenarios, though not to benefit all stakeholders. Further, they found higher price convergence, indicating more efficient grid utilization. Mo and Helseth (2012) compared FBMC to CNTC by examining power prices, social welfare, and power flows. They found increased social welfare, higher price convergence, and better grid utilization. Finally, Cui et al. (2021) reviewed FBMC in the Nordics on an overall level. They conducted a minor case study on a sample system of three price areas to illustrate the improved resource utilization with the introduction of FBMC.

A handful of master theses have studied the introduction of FBMC in the Nordics. Jegleim (2015) developed a method for comparison of GSK strategies in the Nordic flow-based project, and Svarstad (2016) elaborated further on the same issue. Nordeng (2016) reviewed alternative approaches for estimating net positions, while Bolkesjø and Rønneseth (2018) investigated the impact on producer surplus for the Nordic hydropower producers. Finally, Brose and Haugsbø (2019) examined the effects of FBMC on the power generators in the NO5 price area. However, none of the theses investigated the benefits of FBMC compared to the current methodology in a study on the complete Nordic power system.

No other relevant articles on FBMC in the Nordics were found, demonstrating the need for more research. The lack of recent publications is noticeable, and even a direct inquiry to Statnett for access to recent, unpublished material on the topic was futile. In contrast, the material covering FBMC in Europe is extensive. The table below lists key findings of relevant literature on FBMC compared to CNTC and nodal pricing in Europe.

Table 3.2: A selection of recent studies on CACM approaches in Europe.

Reference	Scope and conclusion
Bjorndal et al. (2018a)	Study on stylized grid systems for single hours. Identifies increased social welfare at the expense of more congestion and higher re-dispatch costs.
Kristiansen (2019)	Summarizes two years of parallel runs in CWE in 2013-2015. Finds more transfer capacity is made available to the market, increased social welfare and cross-border flows.
Sarfati et al. (2019)	Analyzes imperfect competition in electricity markets under nodal and zonal pricing. Quantifies the efficiency of CNTC, FBMC, and nodal pricing.
Makrygiorgou et al. (2020)	Investigates market coupling in South East Europe. Finds more efficient generation and transmission utilization with FBMC.
Weinhold (2021)	Considers two scenarios for CWE. Commercial exchange capacities are higher, costs are lower, and price convergence increases with FBMC.
Felten et al. (2021)	Derives a stylized model for comparison of FBMC to nodal pricing. Finds large impact of factors such as the selection of GSKs on market results.
Finck (2021)	Studies FBMC in the European Core region. Underlines the impact of congestion management on the welfare distribution between CNTC and FBMC.
Corona et al. (2022)	Studies the impact of introducing more RES in the mix on cross-border congestion and price convergence with the FBMC methodology.
Ovaere et al. (2022)	Estimates the long-term effect of FBMC on cross-border exchanges and price convergence in CWE. Emphasizes the importance of selecting appropriate RAM values.

While the decision to introduce FBMC in Central Europe and the Nordics has been made, there are advocates for a nodal pricing scheme in the European electricity market. Eicke and Schittekatte (2022) summarized the arguments for and against this approach. Nodal pricing is favored for its ability to provide more accurate price signals that reflect the cost of delivering electricity at different locations. This could lead to more efficient use of the transmission network. Additionally, nodal pricing could better integrate renewable sources by incentivizing their placement in the most valuable areas.

However, critics argue that nodal pricing adds complexity in terms of computational demands and the intricacies of price formation and hedging. It could increase the ability of market players to manipulate prices, thus hindering the development of a competitive market. Moreover, it could lead to unequal effects and high consumer prices in certain areas. There is also concern that the price uncertainty introduced by nodal pricing could discourage long-term investments.

Despite these challenges, the potential cost savings of nodal pricing are significant, and Eicke and Schittekatte (2022) recommend reconsidering nodal pricing in the EU and neighboring countries.

3.3 My contributions to the literature

The main objective of this thesis is to develop mathematical models for comparing the two capacity allocation methodologies, CNTC and FBMC, in the Nordic power market in a 2030 scenario with a high share of renewables in the energy mix. The goal is to make an overall assessment of the impact on social welfare, price formation, and congestion management, to enhance our knowledge of the benefits and implications associated with introducing FBMC in the Nordics, because the current literature on this topic is limited.

A proper implementation of the CNTC model requires a price area configuration that ensures that congestion seldom occurs within the price area. The price area design also impacts the flow-based solution domain, and dynamic price areas might be crucial in fully utilizing the FBMC methodology (Bjorndal et al., 2018b). However,

the current price areas are aggregated according to national boundaries and stay unchanged during the market clearing procedures, and bottlenecks may frequently occur within a price area. Voswinkel et al. (2019) evaluate the performance of Flow-Based Market Coupling (FBMC) compared to nodal pricing designs in a real-world setting. They developed a model framework to quantify the welfare of FBMC and found that under ideal circumstances, where price areas are well-configured, FBMC approaches the efficiency of nodal pricing, realizing 87% of the possible gains associated with a nodal pricing scheme. However, the efficiency of FBMC decreases significantly when considering the current European price area configuration, with only 59% of the efficiency of the nodal market design being attained, resulting in societal losses of over 500 million Euros per year.

Another objective of this thesis is therefore to assess the performance of FBMC and CNTC at the nodal level when the price areas are static, and compare the zonal methodologies to an optimal nodal pricing scheme. Specifically, I aim to compare intra-zonal bottlenecks, power flow, and price formation within the pre-defined price areas. To my knowledge, no published articles address this problem in a large-scale study on the entire Norwegian and Swedish power grids.

4 Problem description

This thesis is a part of the project "VannFly - The Value of Grid Information in Flow-Based Market Coupling," conducted by Sintef Energy Research in collaboration with TrønderEnergi and Statnett, among others. The VannFly project aims to identify and analyze the impacts of introducing FBMC into the Nordic system and provide detailed transmission data to market participants.

The scope of this thesis is to summarize relevant literature on the topic of FBMC and incorporate the flow-based market coupling approach into the short-term hydro-thermal scheduling model PriMod. The model will be used for quantitative analyses of the consequences of introducing FBMC in the Nordic power market. The analyses will focus on the impact on social welfare and congestion management, as examined through power flows and prices. A core metric of the European internal energy market is price convergence, because it quantifies increased market efficiency and competition, resulting in lower prices and increased social welfare (Weinhold, 2021). Particular emphasis is therefore put on the degree of price convergence obtained with the two different methodologies in my analyses.

Additionally, this thesis seeks to evaluate the performance of the two methodologies at a nodal level. The evaluation involves allocating the aggregated market solutions to the physical power grid and comparing the resulting power flows and price formations. Moreover, the DC optimal power flow in the system is computed to establish an optimal benchmark and provide insights into how the flow-based solution compares with an optimal nodal pricing scheme.

5 Mathematical model

This chapter presents the PriMod model formulation used for solving the unit commitment and dispatch problem. Section 5.1 provides an overview of decisive assumptions for the model, while Section 5.2 introduces and explains the notation used. Finally, the model formulation is presented in Section 5.3. Two distinct versions of the model, designed for analyzing the two methodologies, are employed in this study. Despite the distinctions, they share the same objective function and overall structure and are presented as one model in this chapter. The last two paragraphs in Section 5.3 contain the CNTC- and FBMC-specific constraints, where the two models diverge.

For comprehensibility and simplicity, only selected parts of the model are presented in this chapter. Omitted elements include constraints and variables related to reservoir and discharge balancing, and options for load curtailment and power dumping. Certain operational restrictions on thermal plants, such as minimum up-and-downtime and ramping requirements, are also excluded. Lastly, this presentation does not include specific technical considerations in the operation of hydropower stations, such as the relation between water discharge and power output. Appendices A and B contain the complete model notation and formulation without these simplifications. The model formulation is based on the formulation from Lyngstad (2022).

5.1 Modeling assumptions

PriMod is a versatile tool with numerous potential configurations. In this study, daily problems are solved at an hourly resolution over a study period of one week, and the model formulation is adjusted accordingly. Power transmission losses are not considered, and the balancing stage is excluded from the model, following Nord Pool's day-ahead market clearing algorithm Euphemia (*Euphemia Public Description*, 2020). To decrease computational time, reserve capacity and limitations on water discharge ramping from hydro modules are not considered.

In the real world, bids and offers are submitted to the power exchange, which creates

supply and demand curves and settles the price, as discussed in Section 2.1. The model in this study takes the water values and thermal plant marginal costs as inputs, which effectively replace the supply curve. Inelastic demand in each area is also given as a parameter. Together with an elastic demand variable, this constitutes the demand curve. FBMC is not implemented throughout the entire system but instead introduced within a synchronous area. A synchronous area is an area with interconnected TSOs sharing a common system frequency. For this study, FBMC is applied within the Norwegian and Swedish areas, where detailed grid information necessary for the implementation is available. Chapter 6 provides further elaboration regarding the input data and the implementation.

5.2 Notation

In this section, the indices, sets, parameters, and variables in the model are presented. Indices and variables are named using lowercase italic letters, while sets are represented by uppercase calligraphic letters, and parameters are denoted using uppercase italic letters. Subscripts are used to denote indices, while superscripts are used to distinguish related variables, sets, or parameters.

Indices

Table 5.1 summarizes the indices used in the model formulation. The index ab refers to the connection's sending and receiving price area.

Table 5.1: Indices.

Index	**Description**	**Index**	**Description**
t	Day	k	Time step
a	Price area	ab	Connection
h	Hydropower module	g	Thermal generating unit
d	Price elastic demand node	c	Cut
w	Week		

Sets

Table 5.2: Sets.

Set	Description
$\mathcal{T}$	Set of days in the study horizon
$\mathcal{K}$	Set of time steps per day
$\mathcal{A}$	Set of price areas
$\mathcal{A}^S$	Set of price areas within the synchronous area, $\mathcal{A}^S \subset \mathcal{A}$
$\mathcal{H}$	Set of hydropower modules
$\mathcal{G}$	Set of thermal generating units
$\mathcal{D}$	Set of price-elastic demands
$\mathcal{D}_a$	Set of price-elastic demands in area a, $\mathcal{D}_a \subset \mathcal{D}$
$\mathcal{L}$	Set of connections
$\mathcal{L}_a$	Set of connections to/from area a, $\mathcal{L}_a \subset \mathcal{L}$
$\mathcal{L}^S$	Set of connections within the synchronous area, $\mathcal{L}^S \subset \mathcal{L}$
$\mathcal{C}$	Set of cuts, the maximum number of iterations
$\mathcal{W}$	Set of weeks for which water values are provided

The sets of the model are presented in Table 5.2. $\mathcal{T}$ includes the set of days in the analysis period. The computational study analyzes one week at a time, i.e., $|\mathcal{T}|$=7. The time resolution of the time steps k in $\mathcal{K}$ is one hour, but each daily problem is solved using a rolling 48-hour horizon; thus $|\mathcal{K}|$= 48. The set of price areas $\mathcal{A}$ includes 57 areas in Europe, while the synchronous area $\mathcal{A}^S$ covers the price areas in Norway and Sweden, where FBMC is introduced in this analysis. $\mathcal{H}$ is the set of hydropower modules in the system. A hydropower module is a water reservoir, with or without production units. $\mathcal{G}$ is all the thermal production plants in the model, while $\mathcal{D}$ contains all nodes with a power demand. The set of connections $\mathcal{L}$ contains the power transmission lines in the model. $\mathcal{C}$ contains Bender's cuts for each week w in $\mathcal{W}$, which is explained in more detail in Section 5.3. Weekly water values are provided exogenously from the long-term model FanSi for every week in $\mathcal{W}$. However, since the study horizon is one week, the set $\mathcal{W}$ contains only the current and previous week.

Parameters

The parameters used in the model are introduced in Table 5.3.

Table 5.3: Parameters.

Parameter	Description
System	
D_{akt}	Price inelastic demand in area a, step k, day t [MW]
P^W_{akt}	Wind production in area a, step k, day t [MW]
C^D_{dkt}	Price of elastic demand d in step k, day t [10^3 €/MWh]
RAM_{abkt}	Remaining available margin on connection ab [MW]
ATC_{ab}	Available transfer capacity on connection ab [MW]
$PTDF^{a'}_{abkt}$	PTDF on connection ab from area a'
T_t	Numerical value of day t, T_t = [1, 2, ..., 7]
W	The week for which the problem is solved
Hydropower	
B_{wc}	Constant value in the cost function for week w, cut c [10^3 €]
Π_{hwc}	Cut coefficient for module h, week w, cut c [10^3 €/Mm^3]
C^S_{hkt}	Start-up cost of hydro module h, step k, day t [10^3 €/MW]
u_{h01}	Initial unit commitment status for module h [binary]
$\underline{P}_h$, $\bar{P}_h$	Min and max production capacity of module h [Mm^3]
Thermal power	
C^G_{gkt}	Marginal cost of thermal unit g, step k, day t [10^3 €/MWh]
C^S_g	Start-up cost of thermal unit g [10^3 €]
u_{g01}	Initial commitment status of thermal unit g [binary]
$\underline{P}_{gkt}$, $\bar{P}_{gkt}$	Min and max production capacity of unit g, step k, day t [m^3/s]

D_{akt} and P^W_{akt} represent constant power demand and production in each area and time step, while C^D_{dkt} is the price of the variable power demand within each area and time step. The parameters RAM_{abkt}, ATC_{ab}, and $PTDF^{a'}_{abkt}$ are explained in detail in Chapter 2, and the determination of the time-dependent PTDF and RAM values employed in the model are described in Chapter 6. Since water values are

provided weekly, T_t represents the numerical value of each day in the week, for computing a weighted daily valuation of stored water. B_{wc} and Π_{hwc} are provided from the long-term model FanSi and used for water valuation. B_{wc} contains the right-hand sides, and Π_{hwc} the coefficients of linear cut constraints resulting from a Bender's decomposition of the long-term hydropower scheduling problem. The remaining parameters are the plants' start-up costs and production capacities, and the initial condition parameters u_{h01} and u_{g01}, stating whether or not the plants are in operation at the beginning of the analysis period.

Variables

The decision variables in the model are listed in Table 5.4.

Table 5.4: Variables.

Variable	Description
System	
y^D_{dkt}	Amount of price elastic demand d covered in step k, day t [MW]
f_{abkt}	Power flow on connection ab, step k, day t [MW]
np_{akt}	Net position in area a, step k, day t [MW]
Hydropower	
r_{hkt}	Reservoir level at module h, step k, day t [Mm^3]
p_{hkt}	Production at module h, step k, day t [MW]
u_{hkt}	Unit commitment status for module h, step k, day t [binary]
c^S_{hkt}	Start-up cost paid for module h, step k, day t [binary]
α^W_w	Future cost of hydropower operation from week w [10^3 €]
α_t	Future cost of hydropower operation from day t [10^3 €]
Thermal power	
p_{gkt}	Power generation at thermal unit g, step k, day t [MW]
u_{gkt}	Unit commitment status for unit g, step k, day t [binary]
w_{gkt}	Start-up at unit g, step k, day t [binary]
z_{gkt}	Shut-down at unit g, step k, day t [binary]

Most of the listed variables are self-explanatory, perhaps except the future cost

variables. α_w^W is the cost-to-go function of operating the system from the end of week w and is determined based on the cuts from FanSi. α_t is the weighted daily value of α_w^W in the current and previous week.

5.3 Model formulation

Objective function

$$\begin{aligned} \min z = \sum_{k \in \mathcal{K}} \Bigg(\sum_{g \in \mathcal{G}} \left(C_{gkt}^G p_{gkt} + C_g^S w_{gkt} \right) \\ - \sum_{d \in \mathcal{D}} C_{dkt}^D y_{dkt}^D + \sum_{h \in \mathcal{H}} c_{hkt}^S \Bigg) + \alpha_t, \qquad t \in \mathcal{T} \end{aligned} \tag{5.1}$$

The objective function (5.1) minimizes daily system costs associated with the unit commitment and dispatch of the hydro- and thermal power plants, for each day t in the study horizon. The first two terms, $C_{gkt}^G \cdot p_{gkt}$ and $C_g^S \cdot w_{gkt}$, are operating and start-up costs of the thermal generation. The third term, y_{dkt}^D, is the price elastic demand covered and sold at a price C_{dkt}^D. The fourth term, c_{hkt}^S, is the hydropower start-up costs, while the last term, α_t, is the expected cost of operating the hydro modules.

Hydropower constraints

Water valuation:

$$\alpha_w^W - \sum_{h \in \mathcal{H}} \Pi_{hwc} r_{hkt} \geq B_{wc}, \qquad w \in [W-1, W],\ t \in \mathcal{T},\ c \in \mathcal{C},\ k = |\mathcal{K}| \tag{5.2}$$

Equation 5.2 values the available water, i.e., the sum of all reservoir levels r_{hkt}, in the system at the end of each day. B_{wc} and Π_{hwc} represent the right-hand side and coefficients of the Bender's cuts, computed in the long-term model FanSi, while α_w^W is the future cost of operating the hydro modules from the end of week w. This water valuation procedure follows Diniz and Souza (2014). See also the background theory section 2.5 for further elaborations on the water values. A simple illustration of the cut constraints is presented in Figure 5.1 below.

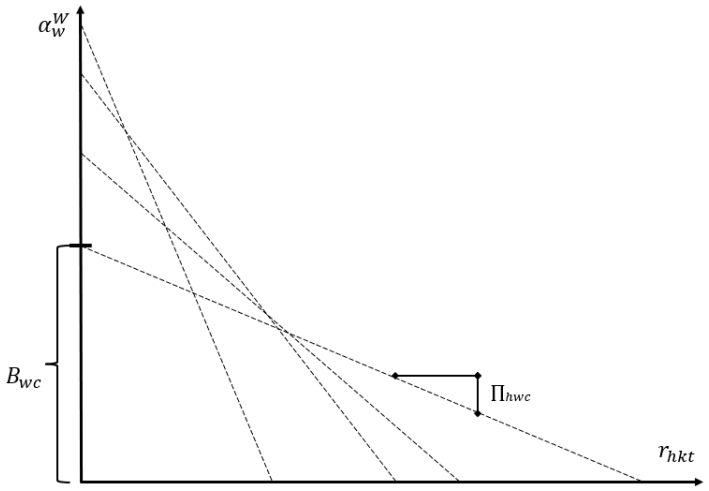

Figure 5.1: Illustration of the Bender's cuts from FanSi (Helseth et al., 2018).

While the Bender's cuts represent weekly water valuations, our problem requires daily solutions. To account for this, we calculate the daily value, α_t, by interpolating the cost-to-go functions, α_w^W, for the current and previous week, as shown in Equation 5.3.

$$\alpha_t = \frac{T_t}{|\mathcal{T}|}\alpha_w^W + (1 - \frac{T_t}{|\mathcal{T}|})\alpha_{w-1}^W, \qquad w = W,\ t \in \mathcal{T} \tag{5.3}$$

In addition to water valuation constraints, Equation 5.4 defines hydropower plant start-up costs c_{hkt}^S based on unit commitment u_{hkt} and start-up cost C_h^S. Equation 5.5 restricts the power generation p_{hkt} to its minimum and maximum values and logically connects the unit commitment variable of every hydro module to its power output. Note that u_{h01} is defined as an input parameter and that for $t > 1$, the index $k-1$ points to the last time step of the previous day.

$$c_{hkt}^S \geq C_h^S\big(u_{hkt} - u_{h,k-1,t}\big), \qquad h \in \mathcal{H},\ k \in \mathcal{K},\ t \in \mathcal{T} \tag{5.4}$$

$$u_{hkt}\underline{P}_h \leq p_{hkt} \leq u_{hkt}\bar{P}_h, \qquad h \in \mathcal{H},\ k \in \mathcal{K},\ t \in \mathcal{T} \tag{5.5}$$

Thermal constraints

Equations 5.6 and 5.7 provide the logical connections between unit commitment u_{gkt} and the start-up and shut-down variables w_{gkt} and z_{gkt} of the thermal units.

Equation 5.8 restricts power generation and connects unit commitment u_{gkt} to power output p_{gkt}. Again, u_{g01} is defined as an input parameter.

$$u_{g,k-1,t} - u_{gkt} + w_{gkt} - z_{gkt} = 0, \qquad g \in \mathcal{G},\ k \in \mathcal{K},\ t \in \mathcal{T} \tag{5.6}$$

$$w_{gkt} + z_{gkt} \leq 1, \qquad g \in \mathcal{G},\ k \in \mathcal{K},\ t \in \mathcal{T} \tag{5.7}$$

$$u_{gkt}\underline{P}_{gkt} \leq p_{gkt} \leq u_{gkt}\bar{P}_{gkt}, \qquad g \in \mathcal{G},\ k \in \mathcal{K},\ t \in \mathcal{T} \tag{5.8}$$

CNTC specific constraints

Power balance:

$$\begin{aligned} \sum_{h \in \mathcal{H}} p_{hkt} + \sum_{g \in \mathcal{G}} p_{gkt} - \sum_{d \in \mathcal{D}_a} y^D_{dkt} + \sum_{(a,b) \in \mathcal{L}_a} \left(f_{bakt} - f_{abkt}\right) \\ = D_{akt} - P^W_{akt}, \qquad a \in \mathcal{A},\ k \in \mathcal{K},\ t \in \mathcal{T} \end{aligned} \tag{5.9}$$

Equation 5.9 ensures that in each area a, the generated hydro and thermal power p_{hkt} and p_{gkt}, added to the net exchanged power with neighboring areas $f_{bakt} - f_{abkt}$, covers the sum of elastic and inelastic area demand (y^D_{dkt} and D_{akt}), subtracted any wind power generation P^W_{akt}. Finally, Equation 5.10 restricts the power flow f_{abkt} on each line to the available transfer capacity ATC_{ab}.

$$0 \leq f_{abkt} \leq ATC_{ab}, \qquad (a,b) \in \mathcal{L},\ k \in \mathcal{K},\ t \in \mathcal{T} \tag{5.10}$$

FBMC specific constraints

With FBMC, the power balance constraints apply only outside the synchronous area:

$$\begin{aligned} \sum_{h \in \mathcal{H}} p_{hkt} + \sum_{g \in \mathcal{G}} p_{gkt} - \sum_{d \in \mathcal{D}_a} y^D_{dkt} + \sum_{(a,b) \in \mathcal{L}_a} \left(f_{bakt} - f_{abkt}\right) \\ = D_{akt} - P^W_{akt}, \qquad a \in \mathcal{A} \backslash \{\mathcal{A}^S\},\ k \in \mathcal{K},\ t \in \mathcal{T} \end{aligned} \tag{5.11}$$

In the synchronous area, the power balance is expressed with the net position variable, np_{akt}. The sum of net positions in a synchronous area is always zero, as stated in Equation 5.13. Thus, the area net position cannot be defined simply as generation

subtracted demand; power flows to or from areas outside the synchronous area must also be included in the definition presented in Equation 5.12.

$$\begin{aligned} np_{akt} = &\sum_{h \in \mathcal{H}} p_{hkt} + \sum_{g \in \mathcal{G}} p_{gkt} - \sum_{d \in \mathcal{D}_a} y^D_{dkt} \\ &+ \sum_{\substack{(a,b) \in \mathcal{L}_a \\ b \notin \mathcal{A}^S}} \left(f_{bakt} - f_{abkt} \right) - D_{akt} + P^W_{akt}, \qquad a \in \mathcal{A}^S,\ k \in \mathcal{K},\ t \in \mathcal{T} \end{aligned} \tag{5.12}$$

Equation 5.14 defines the power transmission on every connection ab, using the flow-based definition discussed in Section 2.2. Finally, Equation 5.15 limits the power flow to the remaining available margin on the transmission line.

$$\sum_{a \in \mathcal{A}^S} np_{akt} = 0, \qquad k \in \mathcal{K},\ t \in \mathcal{T} \tag{5.13}$$

$$f_{abkt} = \sum_{a' \in \mathcal{A}^S} PTDF^{a'}_{abkt} \cdot np_{a'kt}, \qquad (a,b) \in \mathcal{L}^S,\ k \in \mathcal{K},\ t \in \mathcal{T} \tag{5.14}$$

$$0 \leq f_{abkt} \leq RAM_{abkt}, \qquad (a,b) \in \mathcal{L}^S,\ k \in \mathcal{K},\ t \in \mathcal{T} \tag{5.15}$$

6 Data and implementation

The first section of this chapter presents the data sets that underpin the analyses in this thesis, as well as the modifications made to ensure their applicability. The second section describes the DC power flow computation, the implementation of FBMC in PriMod, and finally, the optimal power flow model. The first part of Section 6.1 derives from Chapter 8 of Lyngstad (2022).

6.1 Data set description

The data set "HydroCen Low Emission scenario" was developed by HydroCen and Sintef Energy Research in collaboration with various Nordic energy industry stakeholders. Influenced by NVE's and Statnett's long-term market analyses, this data set embodies a 2030 scenario for the European power system (Haugen and Schäffer, 2020) and forms the input for the PriMod analyses.

Furthermore, the power flow analyses utilize a data set from NVE, which details the power transmission infrastructure in Norway and Sweden. This section elaborates on these two data sets.

6.1.1 Grid topology

The grid model from the HydroCen data set represents the power system connections between the Nordic countries, Great Britain, the Baltics, and core European countries, including Germany, Belgium, France, Poland, and the Netherlands. Cross-zonal exchange capacities are aggregated to connect neighboring price areas with appropriate available transfer capacities (ATCs).

For more detailed simulation results, the Norwegian power system is divided into 11 price areas rather than five, reflecting the geographical distribution of power generation and demand. Similarly, the Swedish power system is divided into six price areas. Figure 6.1 illustrates the price areas and cross-zonal connections.

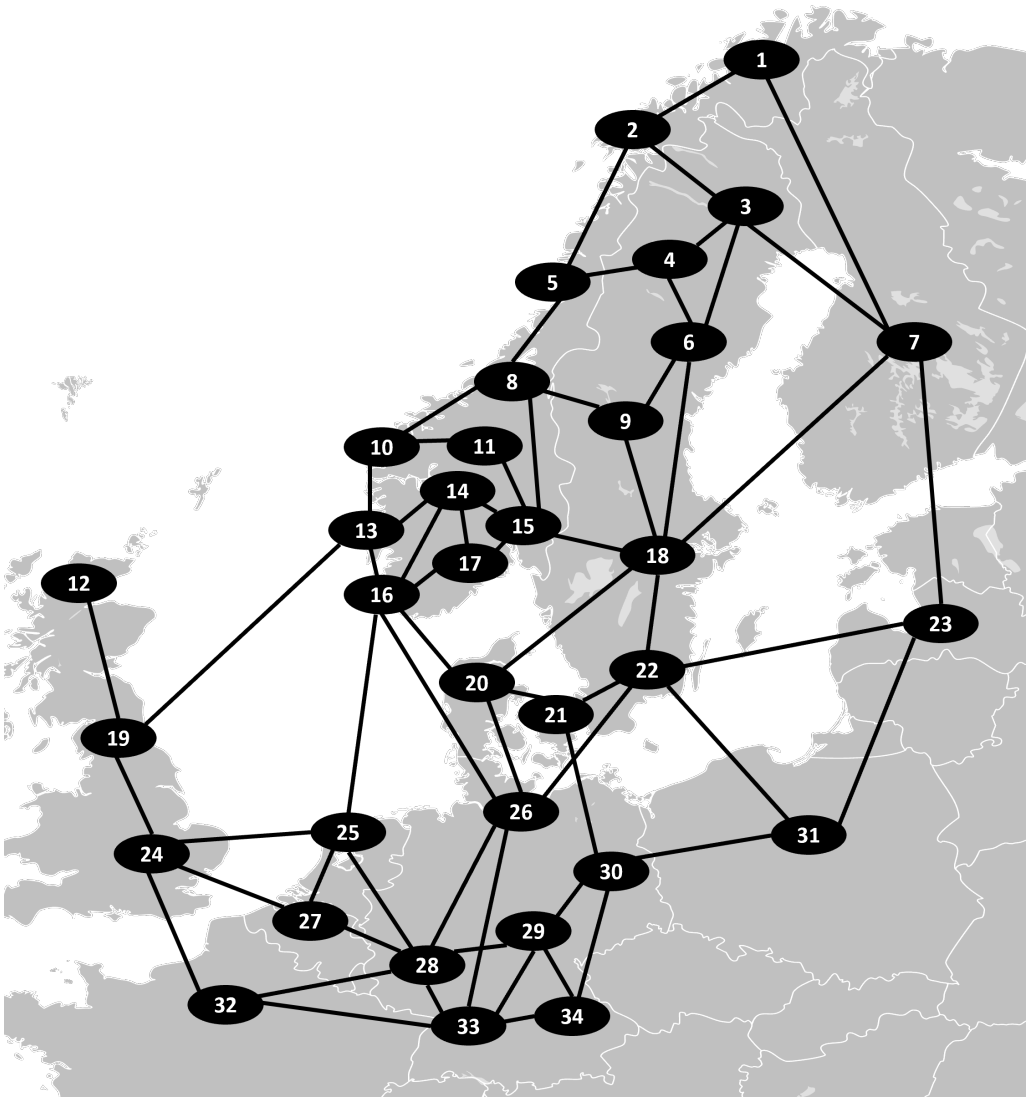

Figure 6.1: Map of the grid used in the analysis.

As described in Chapter 2, the power transfer distribution factors (PTDFs) are calculated utilizing the line reactances that comprise the Y_{DC} matrix. This information stems from the detailed grid description provided by NVE, which is only available for the Norwegian and Swedish parts of the system. As a result, the PTDFs can only be determined for these regions, designating the 17 areas in Norway and Sweden as the synchronous area where FBMC is implemented in the model.

Determining the appropriate ATCs is a complex task. The difficulty involves finding a balance: setting a capacity too high may result in infeasible flows, whereas a low capacity could needlessly limit the power system. The ATCs for the connections between price areas are defined in the HydroCen Low Emission scenario, based

on operational experience and historical data. These values represent the thermal capacity of existing power transmission lines while maintaining adequate security margins to prevent overloads. Several connections in the data set have ATCs significantly below the aggregated thermal capacity, some even lower than 20% of the thermal capacity. Section 6.2 delves into the RAM value calculation for these connections.

6.1.2 Power generation and demand time series

The HydroCen data set includes Hierarchical Data Format (HDF) files comprising detailed time series of hydrological data, weather conditions, and load profiles in Europe from 1980 to 2010. This thesis focuses on the weeks from the 2010 time series. The load profiles in the data set have been scaled to project realistic values for 2030. While some parts of the data set are classified, Table 6.1 gives a sense of the power system's magnitude in the model, exhibiting the annual electric power demand of different countries.

Table 6.1: 2010 scaled power demand, aggregated from zonal to national values.

Country	Demand [TWh]	Country	Demand [TWh]
Norway	134.89	Sweden	142.67
Denmark	39.39	Finland	90.90
Great Britain	358.76	Germany	605.22
France	513.78	Netherlands	121.01
Belgium	86.53	Poland	181.88
Baltics	29.08		

The weather data includes initial water reservoir volumes, hydro inflow, and wind speed data. The data set also includes thermal marginal costs, production capacities, and start-up costs for all hydro modules and thermal plants, all provided at an hourly resolution. Figure 6.2 displays Norway's total electric power demand for 2010, scaled to 2030 values.

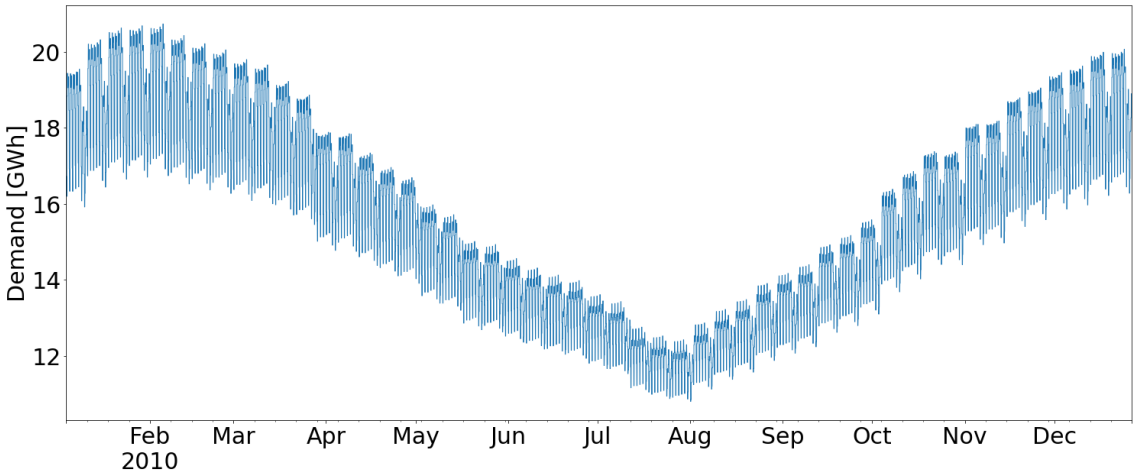

Figure 6.2: 2010 scaled Norwegian power demand time series.

6.1.3 Detailed grid description

Norges vassdrags- og energidirektorat (NVE) supplies the detailed grid description used in the power flow analysis. This data set includes information about nodes, transmission lines, and transformers in Norway and Sweden. Tables 6.2 and 6.3 provide an overview of the data set's structure.

Table 6.2: Node data.

Node	V_{nom} [kV]	lat	lon
1072	420	8.93242	63.67577

Table 6.3: Transmission line data.

Node	Node	V_{nom} [kV]	r [Ω]	x [Ω]	c [μF]	P_{max} [MW]
1072	1080	420	1.32	23.69	0.424	3088

The data set also houses transformer data provided in a similar fashion and includes over 2000 nodes and more than 1000 transmission lines and transformers. Below is a geographical illustration of the Norwegian nodes and transmission lines.

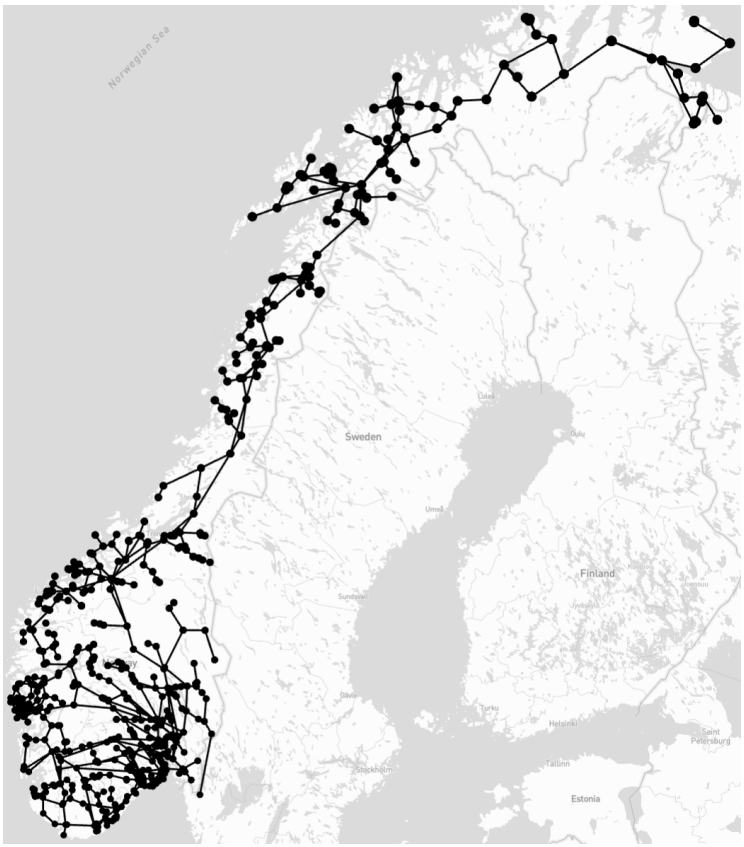

Figure 6.3: Map of the detailed Norwegian grid description (*NVE-Atlas*, 2023).

6.1.4 Coupling files

The HydroCen data set contains aggregated zonal values to simplify the system's representation. The resulting PriMod output offers information on zone-to-zone power flow, hydro module generation and reservoir balance, thermal generation, and wind power. Coupling files are required to convert these aggregated values to nodal net positions and transmission line flows.

Sintef Energy Research has developed coupling files that assign thermal and hydropower generation capacities to specific nodes. Furthermore, these files distribute the firm power demand of an area to nodes within that area and delegate power imports and exports from regions outside the detailed grid description to specified nodes. However, a suitable area wind power allocation was not readily available. To address this, I utilized public information available at *NVE-Atlas* (2023) to develop an appropriate wind power allocation for the price areas.

Table 6.4 shows an example demonstrating the structure of the coupling files.

Table 6.4: Coupling files.

Hydro module coupling			Firm power coupling		
Module	Node	Share	Area	Node	Share
302	1072	10	1	1072	10
302	1082	20	1	1082	15
405	1905	10	1	1092	12
607	1782	10	2	1092	20

6.2 Implementation

The model implementation is divided into three parts: a DC power flow calculation in pandapower, the flow-based formulation of PriMod in Pyomo, and an optimal power flow computation with PowerModels.

6.2.1 Power flow analysis in pandapower

Nodal PTDFs can be calculated provided the line reactances of the connections in the system. Furthermore, with an appropriate GSK strategy, we can compute zonal PTDFs. However, computing RAM values also require nodal net positions, as indicated by Equation 2.17 in Chapter 2, which is repeated below for convenience:

$$F_{ij}^{ref'} = \underbrace{\sum_{n} ptdf_{ij}^{n} \cdot NP_n}_{physical\ flow\ F_{ij}^{ref}} - \underbrace{\sum_{a} ptdf_{ij}^{a} \cdot NP_a}_{market\ flow}$$

Therefore, a DC power flow computation is necessary to obtain RAM values for the flow-based formulation of PriMod. This thesis conducts power flow analyses using *pandapower* (Thurner et al., 2018), an open-source power system analysis tool designed for static analysis and optimization of balanced power systems. This tool offers various functionalities, including DC-approximated power flow and optimal power flow tools.

Pandapower employs a tabular data structure based on the Python library *pandas* for defining networks, which facilitates user-friendly handling of input and output

parameters, beneficial for analyzing large networks. The implementation in Python makes pandapower accessible and allows easy integration with third-party libraries like the Julia-based optimization tool *PowerModels* (Coffrin et al., 2018), used for solving the OPF problem in this thesis.

The pandas library can store variables of any data type within a single dataframe, including electrical parameters, status variables, and metadata such as names and descriptions. Network components are represented in tables containing all parameters of a specific element, alongside a power flow result table. Users can customize these tables by adding new columns without affecting the functionality of pandapower. All inherent pandas methods can be used for efficient access and analysis of the network and result data. A pandapower network is essentially a Python dictionary housing all the network information, depicted in Figure 6.4.

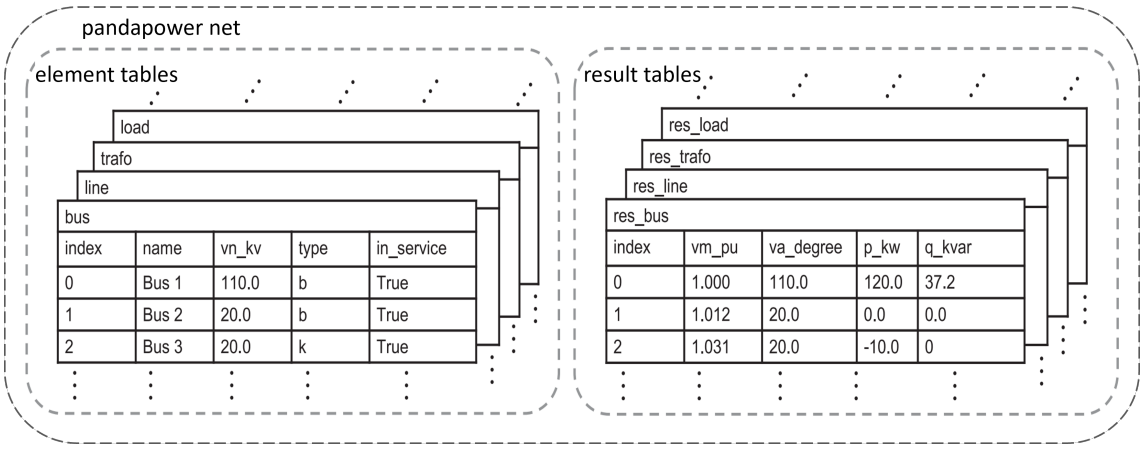

Figure 6.4: Schematic overview of the network representation (Thurner et al., 2018).

Raw system data provided by NVE and coupling files developed by Sintef were cleaned and stored in pandas dataframes, making them suitable for building a pandapower network. Pandapower's built-in network diagnosis functions assisted in building a complete and converging network, providing logging output and diagnoses with adjustable detail levels to check for common issues leading to errors.

Given a complete pandapower network, the nodal DC power flow solution corresponding to the PriMod market solution can be computed for a specific time step. From the power flow solution, we can determine the RAM values of each connection. This process is illustrated in Figure 6.5, exemplified using price area one (Finnmark).

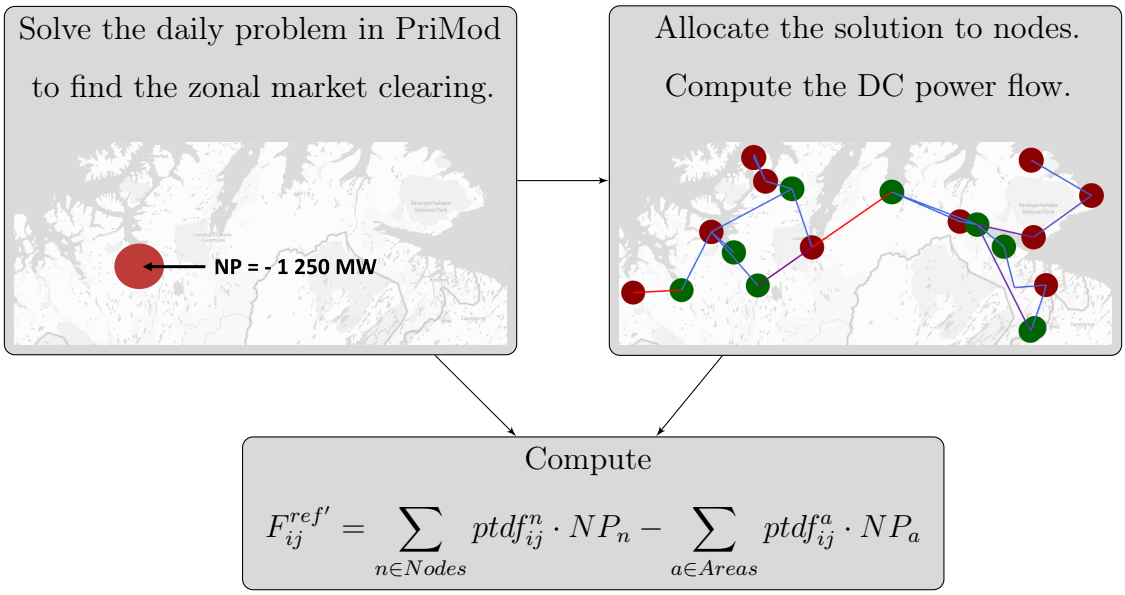

Figure 6.5: Flowchart showing the zonal-nodal interaction.

6.2.2 FBMC in PriMod

The model formulation from Chapter 5 was implemented in Lyngstad (2022) in Pyomo, a Python-based optimization tool with agile formulation resources. The implementation was based on the previously developed CNTC model formulation of PriMod. This thesis extends the implementation with a detailed grid description, allowing for the computation of endogenous PTDFs and time-dependent RAM values.

The RAM values are determined iteratively throughout the solution process. Initially, the daily problems are resolved using the equation

$$RAM_{ij} = F_{ij}^{max} - FRM_{ij}$$

to find a reference state of the system. F_{ij}^{max} is the thermal capacity of the cross-zonal connection, which is calculated by summing up the thermal capacities of all transmission lines connecting areas i and j in the detailed grid description. As mentioned in Chapter 2, EU regulations require that 70% of the thermal capacity be available to the market. Therefore, the Flow Reliability Margins (FRMs) are set to 30% at every connection ij.

Figure 6.5 above illustrates how the production dispatch from the initial solution is

allocated to the nodes and how $F_{ij}^{ref'}$ is computed. Subsequently, the daily problem is resolved using

$$RAM_{ij} = F_{ij}^{max} - FRM_{ij} - F_{ij}^{ref'}$$

The flowchart below displays a brief overview of the steps involved in implementing FBMC in PriMod.

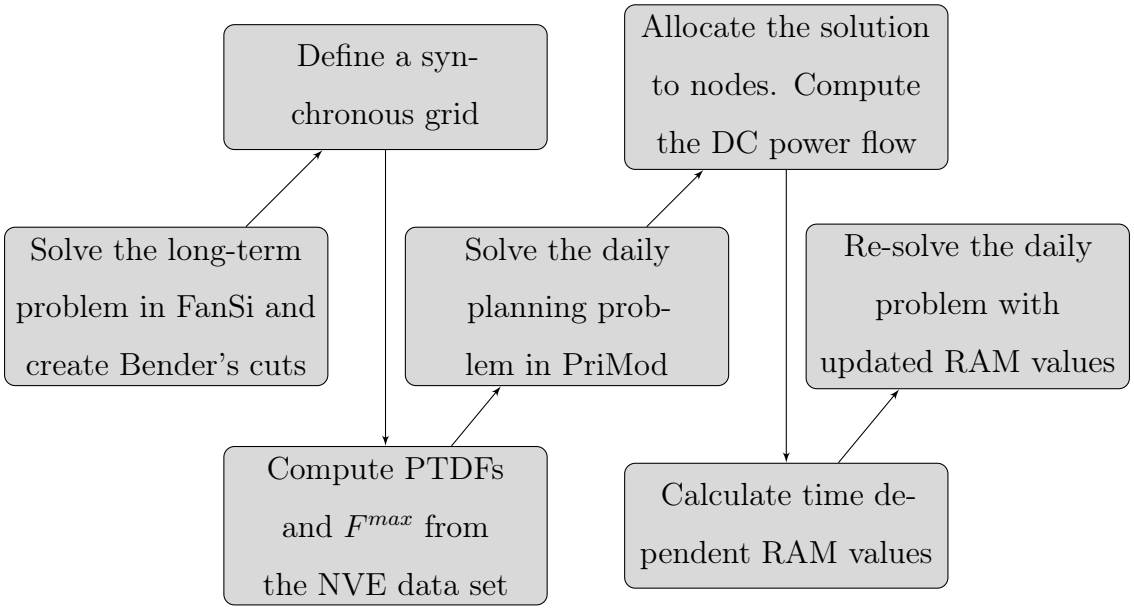

Figure 6.6: Flowchart showing the procedural steps in the implementation.

6.2.3 Optimal power flow with PowerModels.jl

Pandapower's element-based data structure allows the configuration of costs, flexibilities, and constraints for solving optimal power flow (OPF) problems. The network used for the DC Power flow is augmented with generator costs, power output constraints, and transmission line capacities for the OPF calculation.

Each generator and load's cost function is characterized by a piecewise linear cost function of their power output. The marginal costs of the hydro modules are the current water values, which are accessible in each time step as the dual value of the reservoir balance constraint (Equation B.2 in Appendix A). The sum of the hydro generation allocated to a specific node from several hydro modules was merged into a single generator within the DC power flow network. This reduced the computational time, but this method does not apply to the OPF network as it would be impossible

to define minimum and maximum generator output constraints for the different modules in the merged hydro generator. Instead, the allocated capacity from a hydro module to a specific node was represented as a unique generator in the network, with its associated marginal cost and output constraints. Thermal generation units have predefined marginal costs for each time step in PriMod, which can be directly entered as cost functions in pandapower alongside output constraints. Price elastic demand is incorporated as loads with negative cost functions and output constraints. Wind power and inelastic demand are included as non-controllable generators and loads with specified output.

Cross-zonal transmission line capacities were reduced to 70% of their thermal capacities to ensure the zonal transfer capacity in PriMod was reflected in the OPF solution. Pandapower interfaces with the optimization tools Pypower and PowerModels.jl. This thesis used PowerModels to solve the model due to its superior convergence properties in large networks (*Optimization with Pypower*, 2023). PowerModels is a Julia-based, open-source framework for power flow evaluations. Drawing inspiration from Matpower, a widely used MATLAB-based power system analysis toolbox, it builds upon JuMP, an optimization package offering a high-level interface for defining optimization problems, including linear programming, mixed-integer programming, and nonlinear problems. PowerModels provides an abstraction layer that captures the structure of mathematical programs for power systems, including power flow equations and network components such as nodes, generators, and connections.

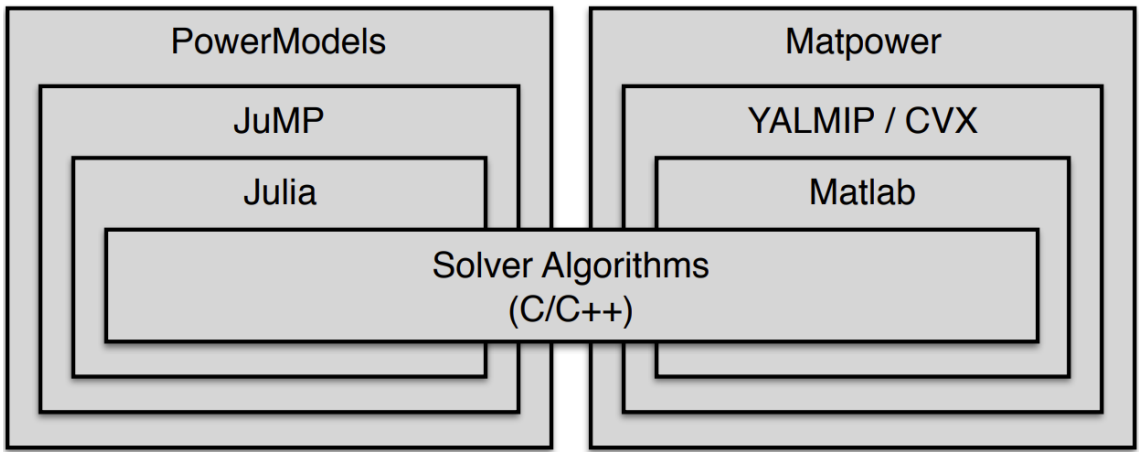

Figure 6.7: Abstraction layers in PowerModels and Matpower (Coffrin et al., 2018)

Figure 6.7 illustrates the abstraction layers in PowerModels and the corresponding layers in the more established Matpower software. The pandapower network is converted to the PowerModels format, solved, and returned with the resulting production dispatch, power flow, and the cost of operating the system at the current time step.

Given the high volume of nodes and branches, pandapower's built-in visualization tools offered unsatisfactory performance. Consequently, the geographic visualization of the results was conducted using *deck.gl* via the Python library *pydeck*. Deck.gl is an open-source WebGL-powered framework that offers interactive and customizable data visualizations on maps, graphs, and charts (OpenJS, 2016a). It supports GPU-accelerated rendering, enabling the smooth handling of large data sets. Pydeck offers a set of Python classes for visualizing large-scale data using deck.gl (OpenJS, 2016b). Users can create custom data visualizations in Python, leveraging deck.gl's rendering capabilities.

The complete data sets and program code are available at Bitbucket, provided authorization from Sintef Energy Research.

7 Computational study

This chapter presents an analysis and discussion of the results obtained from a computational study of the unit commitment and dispatch problem, as outlined in Chapter 5. The test environment is described in Section 7.1. Section 7.2 discusses objective values and congestion management in FBMC and CNTC at the zonal level. The detailed grid analysis is presented in Section 7.3, and finally, Section 7.4 addresses the study's limitations.

7.1 Test environment

Two weeks from the 2010 weather scenario were selected for simulation and analysis to compare the two methodologies. Week six in February (characterized by low temperatures and high demand) and week 27 in July (representing the end of the filling season) were chosen to capture seasonal variations in demand and production patterns effectively.

The detailed grid analysis examines power flow and prices at selected time steps to understand how the market solutions manifest in the physical power grid. Three time steps were selected from each week, focusing on moments when the system was under significant strain. These time steps were chosen based on the cumulative dual values of the PTDF restrictions in the flow-based solution.

The computational specifications are summarized in Table 7.1.

Table 7.1: Hardware and software used in the computational study.

Processor	3 GHz Intel Core i7-1185G7
Memory	32 GB RAM
Programming language	Python v.3.7.12
Commercial solver PriMod	CPLEX v12.10.0
Commercial solver OPF	Ipopt v0.9.1

7.2 CACM comparison with PriMod on zonal level

This section compares FBMC and CNTC using the PriMod model. Evaluations focus on power flows, prices, and congestion management. Key insights are drawn from analyses of aggregated values of congestion rent, grid utilization, and operating conditions during peak constraint periods.

7.2.1 Economic analysis

Table 7.2 presents the aggregated weekly objective values for both weeks, reflecting the operation of the power systems in all the interconnected regions in the HydroCen data set.

Table 7.2: Objective value z [million euros] and computation time t [seconds]. The objective values are inverted, i.e., higher is better.

Week	CNTC		FBMC	
	z [M€]	t [s]	z [M€]	t [s]
6	29 007.75	1 467	29 009.06	2 519
27	45 140.98	1 402	45 142.00	2 443

The objective values include the value of all the stored water in the European power system, which accounts for their large magnitude. Since the end-of-week water valuations are equal, the value of the water reservoirs cancels out. Thus, the magnitude of the improvements in the objective value with FBMC is of greater interest than the relative improvements.

The results indicate that FBMC improves social welfare compared to CNTC; 1.3 M€ in week 6 and 1.02 M€ in week 27. These improvements are consistent with theoretical expectations and underscore the benefits of a more flexible utilization of available exchange capacity. Extrapolating these values, the annual improvement could exceed 50 M€. However, the iterative procedure of computing RAM values means computation time increases significantly with the flow-based approach. Figures 7.1 (a) and (b) depict the progression of the objective values throughout the week.

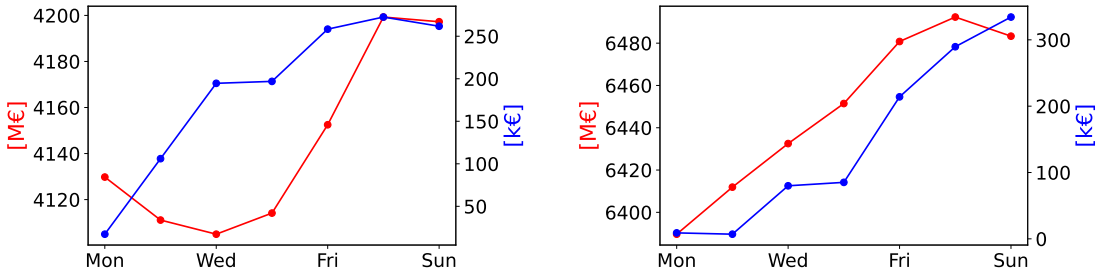

(a) Week 6

(b) Week 27

Figure 7.1: Daily objective values. The left axis and red graph is daily FBMC objective value [M€]. The right axis and blue graph is daily FBMC objective value subtracted daily CNTC objective value [k€].

It is noteworthy that objective value improvements surge towards the week's end. Although the daily problems are solved deterministically, and initial conditions remain the same at the week's start, parameters such as water inflow or wind series are stochastic, and the model is solved with a 48-hour rolling horizon. Despite nearly equal day-one objective values, the day-one solutions with the two approaches differ, and the initial decisions influence subsequent decision spaces. Figures 7.1 (a) and (b) indicate that the value of increased flexibility in the FBMC approach is amplified towards the end of the study horizon, particularly in week 27—a summer week with lower reservoir levels than week six.

7.2.2 Congestion management

The performance of the two methodologies, measured by power flows and prices during periods of system strain, is just as insightful as the objective values. Beyond investigating aggregated values of congestion rent and grid utilization, I also compared snapshots of the operating situation at moments when cross-zonal exchange capacities were most constrained. I identified this time step for each week by considering the sum of the dual values of the transmission capacity constraints. I emphasized the synchronous area in Norway and Sweden, where FBMC was introduced.

Congestion rent

As explained in Chapter 2, congestion rent is revenue collected by the TSO due to congestion in the power grid. It is computed as the price difference between two neighboring areas multiplied by the power flow on the constrained connection.

Table 7.3: The sum of weekly collected congestion rent [€] on the Norwegian and Swedish connections.

Week	CNTC	FBMC
6	509 409.77	138 223.47
27	1 049 159.91	786 293.05

The collected congestion rent is considerably lower with the FBMC approach, indicating a more efficient utilization of available transfer capacity, aligning with theoretical expectations. Moreover, this reduction in congestion rent occurs despite generally larger power flows in the FBMC solution, which indicates improved price convergence. Figure 7.2 presents geographical illustrations of the congestion rents in week six on connections with significant differences between the two CACM approaches.

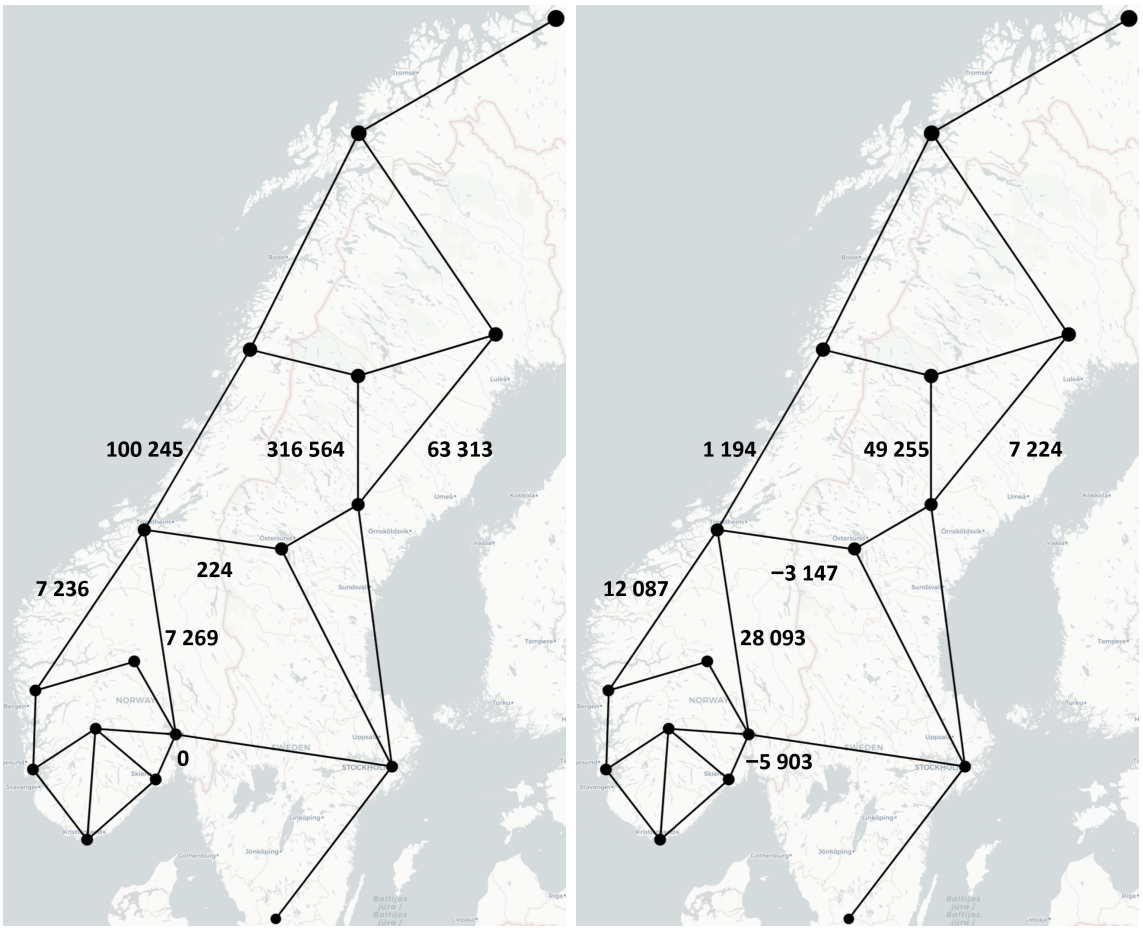

Figure 7.2: Week six aggregated congestion rent [€] with CNTC (left) and FBMC (right) on selected connections.

Worth noting is that the FBMC congestion rent is negative for several connections,

which result from *non-intuitive flows* on the lines. Non-intuitive flows, power flows from high-price to low-price areas, enhance overall social welfare by relieving congestion on constrained connections elsewhere in the system. This is feasible because the flow-based market coupling algorithm permits simultaneous competition for scarce capacity on all connections in the system. In a simplified view, one can perceive the receiving low-price area as a transit area, connecting the sending high-price area to an area with a higher price. This phenomenon does not occur with the CNTC approach, where congestions are handled border by border. Figure 7.3 shows the congestion rent for week 27.

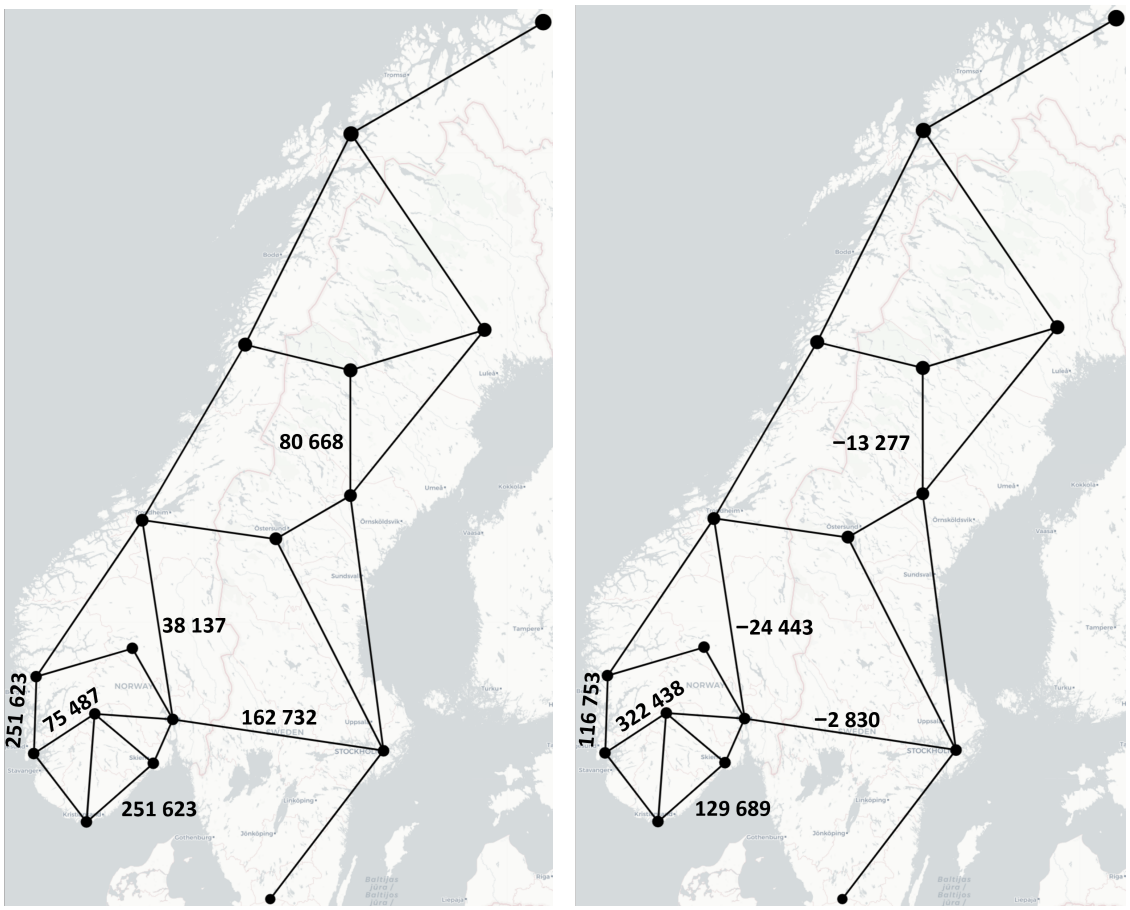

Figure 7.3: Week 27 congestion rent [€] with CNTC (left) and FBMC (right) on selected connections.

In the FBMC solution, non-intuitive flows again reduce total collected congestion rent. The collected rent with CNTC is higher at all connections except the line connecting Telemark to Rogaland, where the FBMC rent is more than four times greater. Rogaland often faces a power deficit due to industry demand and large cities such as Stavanger and Haugesund. In contrast, Telemark has a much lower demand

and substantial installed wind power capacity. As a result, the connection is often congested, and the power exchanged on the connection in the flow-based solution is more than twice the amount exchanged in the CNTC solution.

Power flow

Assessing grid utilization with the two methodologies cannot be done by comparing line loading ($\frac{flow}{capacity} \cdot 100\,\%$), given that the RAM values employed in the FBMC model differ from the ATC values in the CNTC model. Figure 7.4 shows the flow magnitudes and directions for the most congested hour in week six.

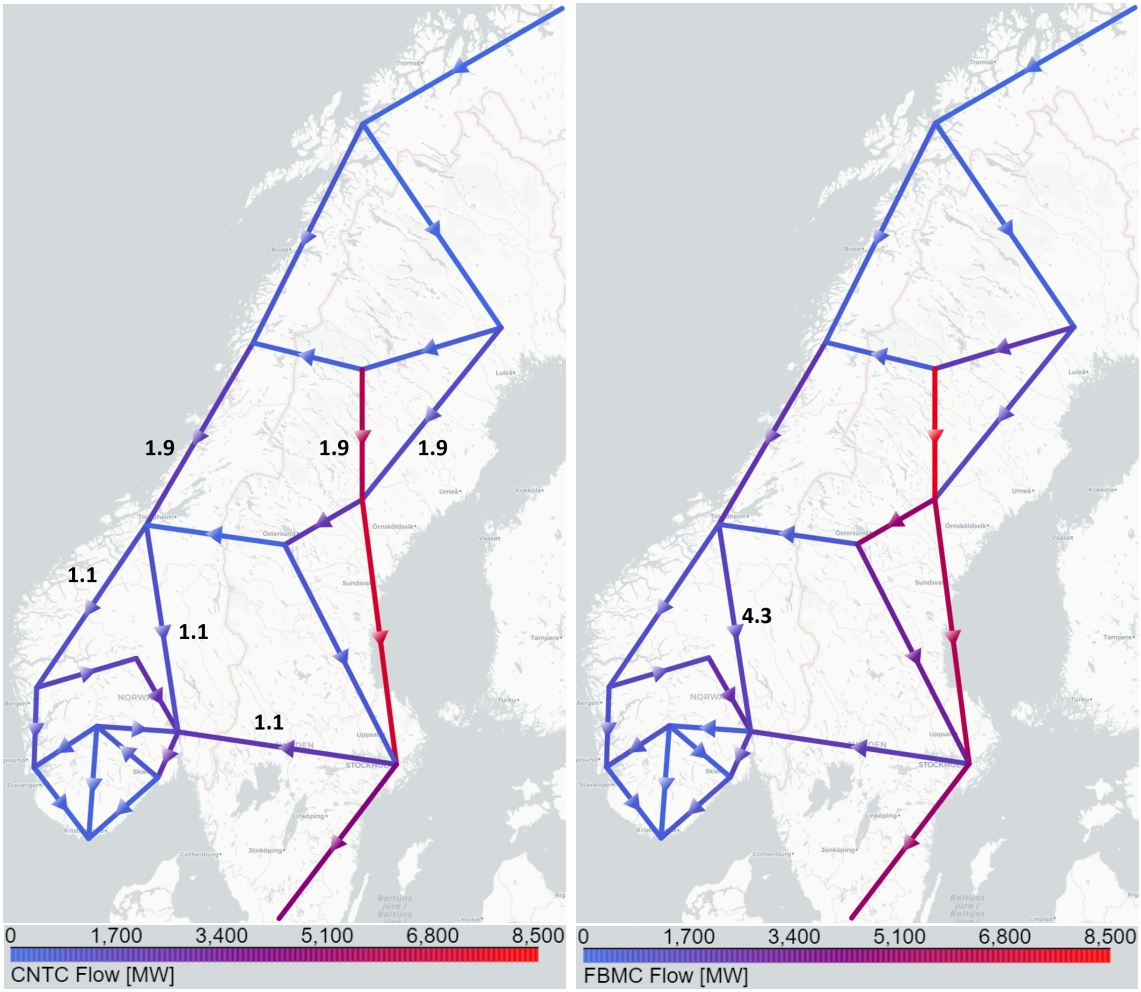

(a) CNTC, Wed. week 6, 02 pm - 03 pm (b) FBMC, Wed. week 6, 02 pm - 03 pm

Figure 7.4: Power flows [MW] and dual values [€/kWh] of the connections.

In the figure, any non-zero dual value of a line's capacity constraint is marked with a bold number next to the line. Dual values in the CNTC solution reflect the price difference between two adjacent price areas with no remaining exchange capacity

between them. Meanwhile, the FBMC dual values mirror the dual value of the PTDF restriction on the connection, dependent on the net positions in all price areas via the PTDFs. Although the connected areas in a given connection usually exert the most significant influence, other areas may significantly impact the flow on certain connections, and thus also the dual value of the PTDF restriction.

The FBMC approach tends to restrict fewer connections, and its dual values are generally higher. This trend is consistent across all time steps and weeks, demonstrating FBMC's ability to identify system-constraining connections. In the flow-based solution, the line from Trøndelag to Oslo is the only connection with a non-zero dual value, illustrating the interdependencies of power flows in a meshed grid. Despite lower prices in the northern areas, this single connection restricts the entire grid, impeding a sufficient north-to-south exchange to equalize the prices.

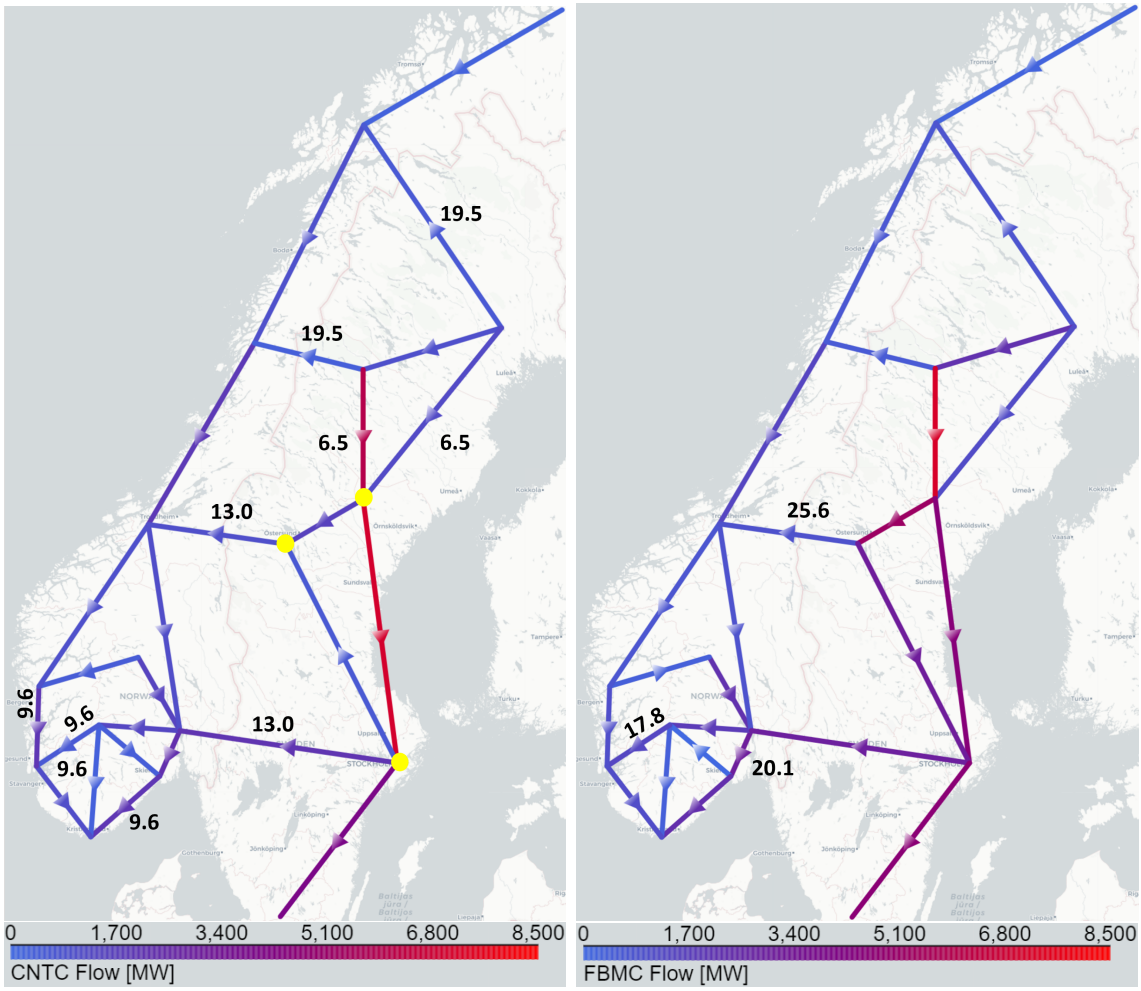

(a) CNTC, Mon. week 27, 01 pm - 02 pm (b) FBMC, Mon. week 27, 01 pm - 02 pm

Figure 7.5: Power flows [MW] and dual values [€/kWh] of the connections.

Figure 7.5 displays the flow magnitudes and directions for the most congested hour in week 27. The pattern concerning dual values reoccurs. Low prices are found in the Swedish areas, while prices in southern Norway are high. In the flow-based solution, the net Norwegian import is 5198 MW, compared to 4055 MW in the CNTC solution, where all lines connecting Norway and Sweden are congested.

Notably, the flow direction changes at several connections, such as the one from Stockholm to Østersund. This happens because flow-based power prices better represent the system's state. In the CNTC solution, the power price is the same in the three areas marked with a yellow dot because none of the triangle's constituent lines are overloaded. With the flow-based approach, the three areas have different prices, even though none of the lines in the triangle are overloaded. The price in Stockholm is highest due to the influence from Oslo's high price, and surplus power in the triangle flows south to Stockholm and west to Norway, limited by the line capacity from Trøndelag to Østersund, not the one from Stockholm to Oslo.

The dual values reflect how the CNTC clearing process offers more freedom border-by-border, but not for the whole system since relaxing a single capacity constraint cannot significantly improve the solution. Unlike FBMC, the CNTC approach does not reveal connections with insufficient capacity. In Figures 7.4 and 7.5, multiple connections constrain the system in the CNTC solution because the capacity constraints are sequentially handled.

Furthermore, the CNTC methodology does not consider physical properties like line reactances, causing significant discrepancies between commercial and physical flows, as discussed in Section 2.2. Quantifying the economic benefits of reducing these deviations by introducing FBMC is challenging, and these benefits are not represented in the model's objective function. Therefore, the actual benefits of the FBMC approach may be understated by the objective values in Table 7.2.

7.3 Detailed grid analysis

The aggregated market solutions were allocated to the physical power grid, as described in Chapter 6. This step was necessary for computing PTDFs and time-dependent RAM values and facilitated a detailed performance assessment of the FBMC and CNTC methodologies at the nodal level. Additionally, an optimal benchmark for comparison was obtained by computing the DC optimal power flow in the system.

As previously mentioned, six time steps with high congestion in the system were selected for a detailed analysis, based on the cumulative dual values of the PTDF restrictions. This section presents the results, including power prices and flows in selected areas of interest.

7.3.1 Economic analysis

Table 7.4: Total power generation costs [€] in the selected time steps.

Time step	CNTC	FBMC	OPF
Week 6, Mon. 06 am - 07 am	1 694 699	1 669 739	1 260 807
Week 6, Tue. 11 pm - 00 am	1 707 284	1 667 040	1 237 885
Week 6, Wed. 02 pm - 03 pm	1 566 234	1 572 284	1 092 863
Week 27, Mon. 01 pm - 02 pm	780 414	787 423	452 455
Week 27, Thu. 01 pm - 02 pm	545 336	588 190	338 924
Week 27, Sun. 07 pm - 08 pm	1 043 131	1 035 956	657 446
The sum of the above time steps	7 337 098	7 320 632	5 040 380

Table 7.4 shows the power generation costs for the selected time steps with FBMC, CNTC, and OPF. The costs associated with FBMC and CNTC vary across different time steps. The total FBMC costs are slightly lower than the CNTC costs, and both zonal pricing schemes result in costs approximately 40% higher than those obtained with OPF.

However, these FBMC and CNTC costs result from a blunt allocation according to

the coupling files of the power generation in each area. Nodal generation derived from the PriMod model lacks detailed information about the underlying cost characteristics at each node. Therefore, comparing the generation costs of the FBMC and CNTC methodologies to evaluate their relative cost-effectiveness is unreliable.

7.3.2 Congestion management

Section 7.2.2 outlined the influence of the CACM methodology on zonal-level congestion management. The detailed grid analysis in this section offers a more comprehensive understanding of congestion patterns and power flows across specific nodes and transmission lines. In addition, comparing snapshots of operational situations during periods of system strain allows us to pinpoint critical congestion hotspots and gain further insight into how the CACM methodology impacts congestion relief within the physical power grid.

Price convergence

Table 7.5: Number of time steps with full price convergence in the synchronous area.

Week	CNTC	FBMC
6	139	144
27	97	97

High price convergence in an integrated electricity market indicates efficient use of the infrastructure and lower system prices. Table 7.5 displays the number of time steps with full price convergence in the synchronous area for CNTC and FBMC during weeks 6 and 27. Theory suggests that FBMC should yield higher price convergence, a notion supported by the data in Table 7.5, albeit with a relatively minor difference. Several time steps characterized by low system congestion saw CNTC prices converging more than the flow-based prices.

Table 7.5 displays the number of time steps with *complete* convergence, where prices are equal in all areas. Minor price variations may occur between adjacent areas with available exchange capacity in the flow-based solution to efficiently relieve congestion

across the entire system. Such variations are unlikely under the CNTC approach, where congestions are handled border by border. Therefore, by lowering the price convergence criterion to 0.1 €/MWh, the FBMC approach further outperforms CNTC in achieving price convergence.

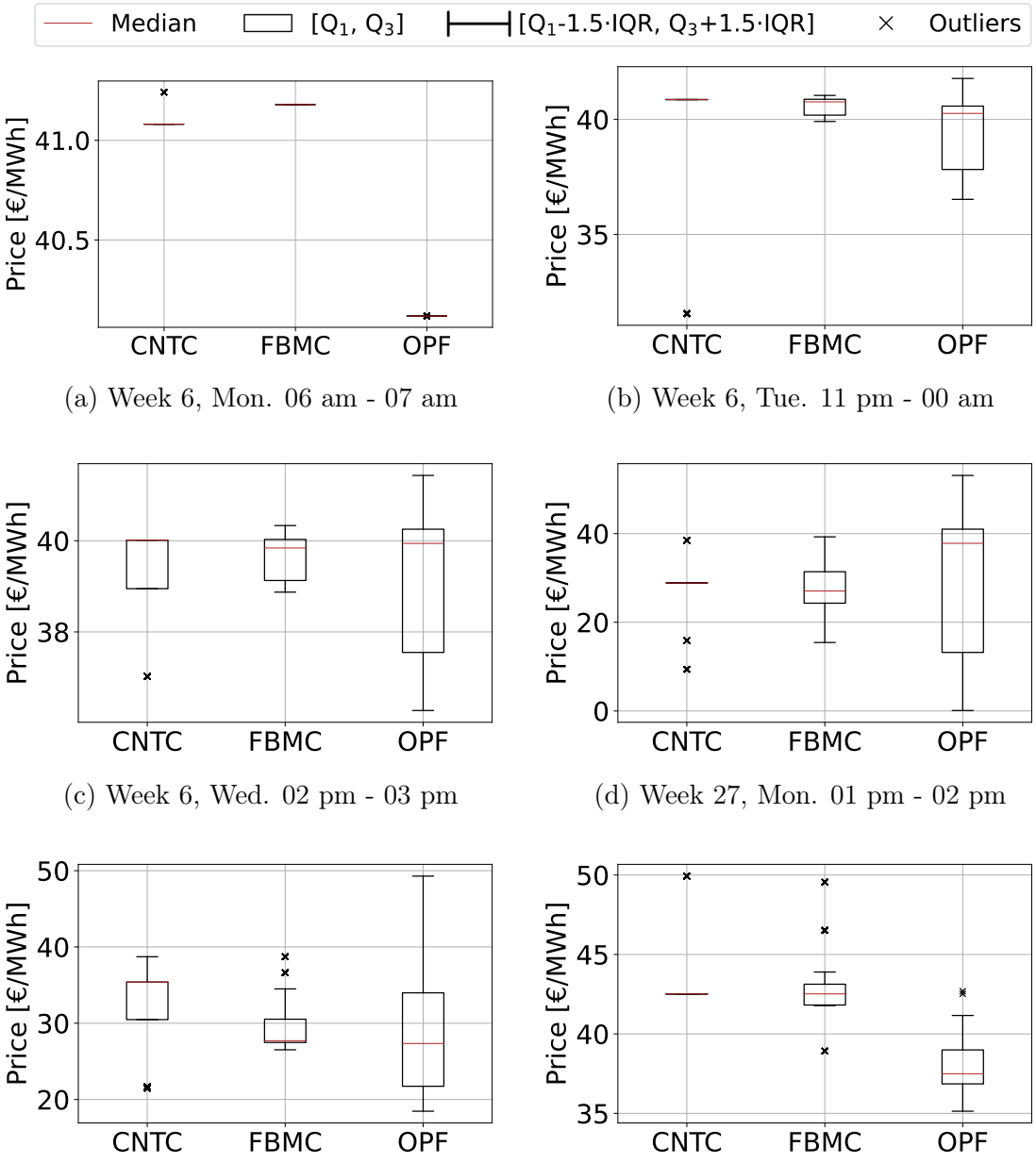

(a) Week 6, Mon. 06 am - 07 am

(b) Week 6, Tue. 11 pm - 00 am

(c) Week 6, Wed. 02 pm - 03 pm

(d) Week 27, Mon. 01 pm - 02 pm

(e) Week 27, Thu. 01 pm - 02 pm

(f) Week 27, Sun. 07 pm - 08 pm

Figure 7.6: Box plot (docs link) of prices [€/MWh] in the synchronous area.

Figure 7.6 illustrates the power prices in the synchronous area, represented by boxplots, for the selected time steps. Bear in mind that in the OPF solution, each node can theoretically have a unique power price, whereas the nodal prices in the

FBMC and CNTC approaches depend on the respective price areas. Thus, outliers in the FBMC and CNTC boxplots indicate the presence of one or more price areas with different prices. A key observation from Figures 7.6 (a) - (f) is that the range of prices determined by the flow-based approach frequently is narrower than that obtained through the CNTC approach.

During congested system conditions, the CNTC approach often produces solutions with near-complete price convergence in most price areas. However, a few areas may experience significantly higher or lower prices. This phenomenon was prevalent during the winter of 2023 when electricity prices for residents in Gudbrandsdalen varied considerably depending on whether they belonged to the NO3 or NO1 price area.

The analysis indicates that the flow-based approach frequently provides solutions with a unique price for each price area, but with smaller price deviations than the CNTC approach. This notion is supported by the boxplot illustration of the prices in Figure 7.6. The flow-based market-clearing approach can reduce the occurrence of extreme price deviations caused by the somewhat arbitrary configuration of price areas, thereby enhancing customers' perceived fairness.

Price formation and power flow

To examine intra-zonal power flows and prices in the flow-based and CNTC solutions, in-depth studies of selected price areas where large internal price deviations occur in the optimal power flow solution are helpful. Such deviations typically arise from substantial wind or solar generation at specific nodes and insufficient intra-zonal transmission capacity. However, these events are not reflected in zonal-level market solutions with uniform prices within each defined price area.

Figures 7.7 (a) and (b) depict the CNTC and FBMC grid utilization in Mid-Norway on Tuesday of week 6, from 11 pm to midnight.

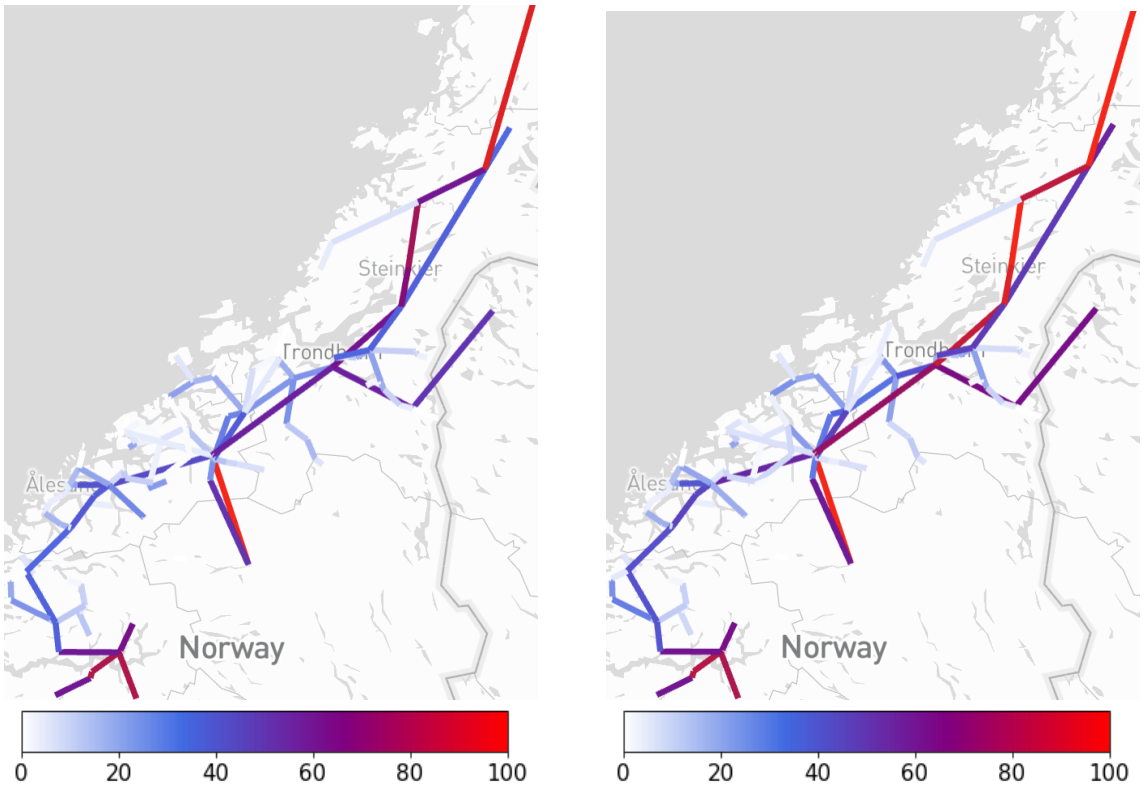

(a) CNTC capacity utilization [%]

(b) FBMC capacity utilization [%]

Figure 7.7: Detailed power flow results in Mid-Norway on Tuesday, week 6, from 11 pm - 00 pm.

To reflect the zonal transfer capacity in PriMod, the capacities of the cross-zonal transmission lines were curtailed to 70% of their thermal capacities in the detailed grid solution, as mentioned in Section 6.2. The capacity utilization in Figure 7.7 is based on these reduced capacities. The CNTC prices in Mid-Norway and Helgeland are €40.86/MWh and €31.56/MWh, respectively, whereas the corresponding FBMC prices are much closer, at €40.18/MWh and €40.07/MWh. The North-to-South grid utilization is higher in the flow-based solution, particularly to the far north, leading to nearly equal area prices in Mid-Norway and Helgeland. This observation is supported by a higher total intra-zonal power flow of 43.6 GW compared to 37.2 GW in the CNTC solution. The total power flow in the system is 239.2 GW (FBMC) and 216.2 GW (CNTC), constituting an overall power flow increase of 10-20% in the FBMC solution.

The pattern of higher quantities of unique prices but smaller price deviations in the flow-based solution is also evident in Figures 7.9 (a), (b), and (c). These figures

depict the OPF, CNTC, and FBMC power prices during a highly congested time step in week 27. The FBMC prices vary more gradually from the high-price areas in South-West Norway to the low-price areas in Sweden, thus aligning more closely with the OPF prices.

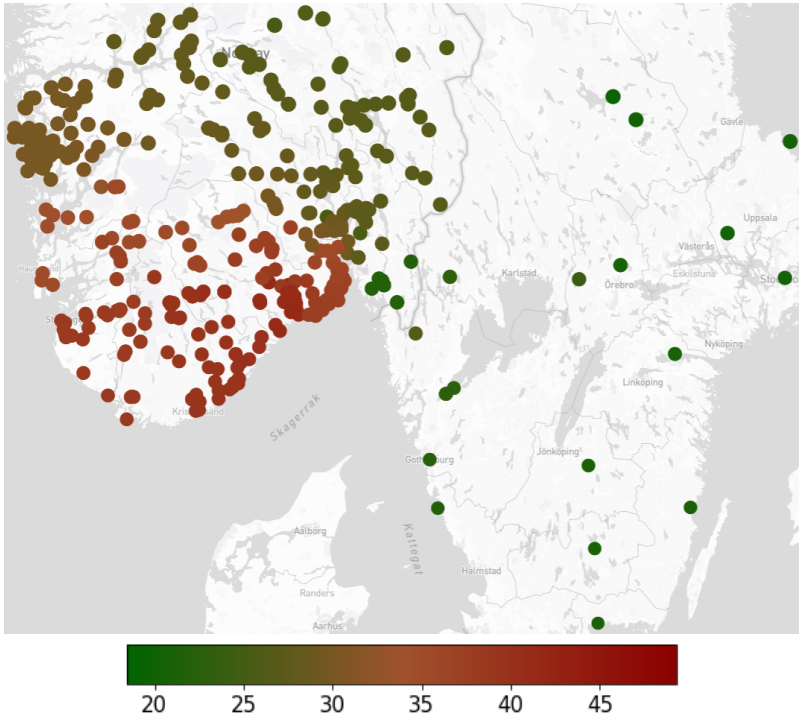

(a) OPF power prices [€/MWh]

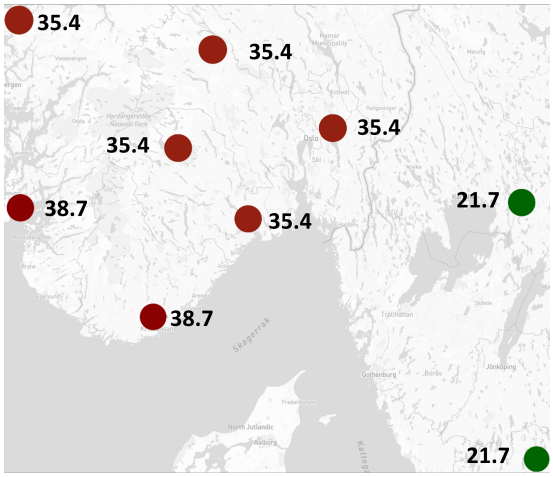

(b) CNTC power prices [€/MWh]

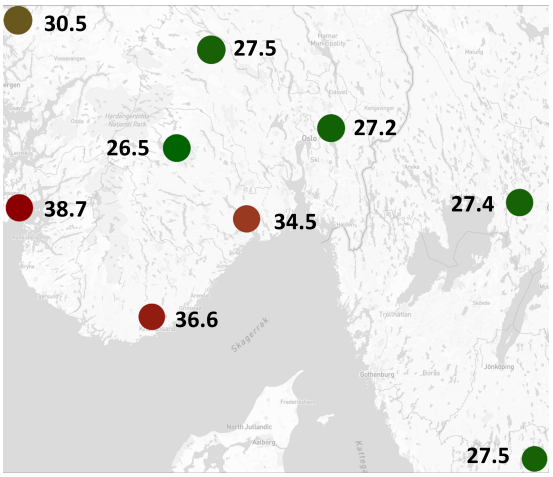

(c) FBMC power prices [€/MWh]

Figure 7.8: Detailed power prices in southern Norway and Sweden on Thursday, week 27, from 01 pm - 02 pm.

In the CNTC model, a noticeable divide in power prices is seen due to insufficient cross-border exchange capacity between Norway and Sweden, resulting in prices in

Oslo nearly doubling the Swedish prices. In contrast, the FBMC solution utilizes more of the physical cross-border transmission capacity, as depicted in Figure 7.9. At this time step, the remaining available margin on the lines connecting Oslo and Sweden significantly exceeds the corresponding available transfer capacity value in the CNTC model, thereby facilitating a more balanced pricing structure between Norway and Sweden. However, the price in Rogaland is also high in the flow-based solution due to insufficient capacity on the line from Telemark to Rogaland. This single connection restricts the system, with a dual value of 19.6 €/kWh (not displayed in the figure). The same connection accounted for more than 40% of the collected congestion rent in week 27, as previously discussed.

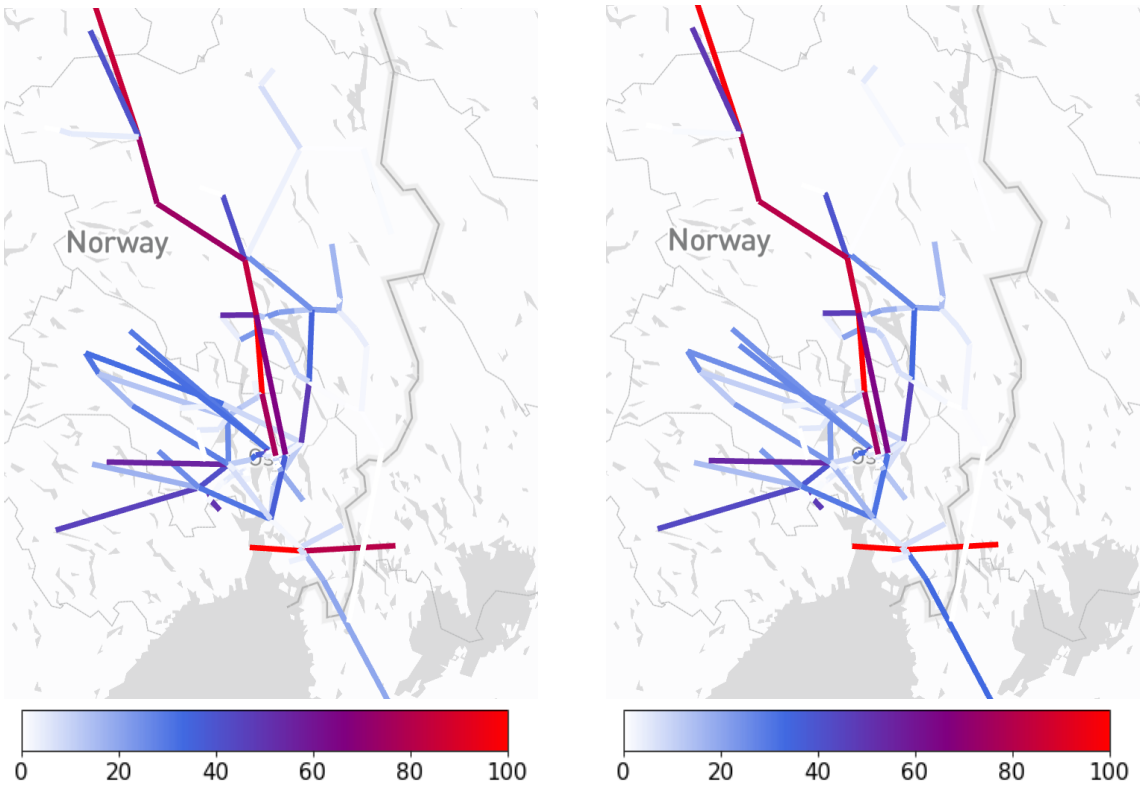

(a) CNTC capacity utilization [%]

(b) FBMC capacity utilization [%]

Figure 7.9: Detailed power flow in the Oslo area on Thursday, week 27, from 01 pm - 02 pm.

7.4 Limitations

This computational study has a few limitations that must be acknowledged. Firstly, the timeframe under consideration is relatively short, necessitating careful extrapolation of the results from isolated weeks and time steps to form general conclusions about the methodologies. The main focus of the study was to study the differences of different market solutions based on snapshots of the system.

Secondly, a uniform GSK strategy was utilized to calculate the PTDFs used in the analysis. Statnett and other Nordic TSOs are exploring more dynamic GSK strategies that will be implemented once FBMC is introduced next year. Furthermore, only selected critical network elements (CNEs) were accounted for—specifically, the transmission lines connecting two price areas. Ideally, the selection of CNEs should be based on the zonal PTDF matrix, operational experience, and robust forecasts for the next day's generation and demand. This is corroborated by studies like Bjorndal et al. (2018a), which demonstrate that improper selection of CNEs can result in high re-dispatch costs in the post-market coupling.

The grid description for Sweden is another limitation of the study. Due to limited public access to this data, the model may not represent the physical grid accurately. Finally, the study is influenced by the stochastic nature of wind and hydro inflow. Along with the rolling horizon approach, this introduces limitations. The initial solution influences the aggregated weekly solution, which the model cannot predict or account for. As a result, differences between the two methodologies tend to accumulate over the week, introducing a level of stochasticity in the results.

8 Concluding remarks and future research

The primary objective of this thesis was to investigate and understand the impact of introducing Flow-Based Market Coupling (FBMC) into the Nordic power market. This objective was driven by the limited existing literature on the implications of this change. In this pursuit, the thesis compared two Capacity Allocation and Congestion Management (CACM) methodologies – the Coordinated Net Transfer Capacity (CNTC) currently in use, and FBMC, the proposed alternative. The European Union has recognized both methodologies as valid approaches to handling electricity transmission across borders, yet they exhibit unique characteristics in their application. Additionally, a nodal pricing approach was studied to get an optimal benchmark.

The study modeled a 2030 scenario for the European power system, utilizing load profiles and weather data from specific weeks in 2010. A detailed comparison between the FBMC, CNTC, and nodal pricing results yielded insights into the influence of these methodologies on power flow patterns and price formations.

The flow-based solution yielded higher objective values than the CNTC solution, indicating improved social welfare. Specifically, the FBMC methodology caused increases of 1.3 million euros in week 6 and 1.02 million euros in week 27. Extrapolated over a year, these improvements could exceed 50 million euros, underscoring the benefits of a more flexible utilization of the available exchange capacity offered by FBMC.

The analysis demonstrated how FBMC and CNTC influence price and flow distributions differently. Notably, the FBMC methodology often resulted in unique prices for each price area, but with smaller price deviations than the CNTC approach. The latter often resulted in near-complete price convergence in most price areas, leading to significant price disparities in a few zones. Furthermore, the collected congestion rent was notably reduced under the flow-based approach, suggesting better grid utilization. Nodal pricing provided an even better system utilization, at the expense of more complexity in the market clearing.

Another noteworthy finding from the study was how the flow-based solution could highlight critical network elements that limit the power flow during periods of strain. Such insights were less apparent in the CNTC solution, suggesting a potential advantage of the FBMC methodology in congestion and grid management.

Despite these promising findings, several limitations, such as the brief timeframe under examination, the implementation of a uniform GSK strategy, and the inherently stochastic nature of wind and hydro inflow, need to be acknowledged. These constraints underscore the need for caution when extrapolating these findings for broader evaluations.

Numerous avenues for future research could provide further insights into the performance and implications of the two CACM methodologies. One is conducting a larger, long-term study to assess the methodologies' relative performances over an extended period spanning several months or years. Furthermore, identifying appropriate critical network elements for which PTDF restrictions are applied poses a challenge. Additional research into this selection process could enhance the accuracy and efficiency of the FBMC approach.

Further research into the effects of specific modifications to the system would be beneficial. This includes exploring the consequences of isolating the contributions from HVDC cables and grouping them into distinct price areas, each with unique PTDF values. Additionally, reducing the size of the price areas to more closely resemble a nodal pricing scheme could significantly impact the market clearing. These adjustments would enable a more accurate representation of the power system and amplify the benefits of the flow-based model, albeit at the cost of increased market clearing complexity.

Lastly, the impact of different GSK strategies on market outcomes is an area for further research. A comprehensive assessment of various GSK strategies is essential for fully harnessing the value of the grid information made available to the market through the flow-based market clearing process.

References

Bjorndal, Endre, Bjorndal, Mette Helene and Cai, Hong (2018a). 'Flow-Based Market Coupling in the European Electricity Market – A Comparison of Efficiency and Feasibility'. *SSRN Electronic Journal*. DOI: 10.2139/ssrn.3272188.

— (2018b). 'The Flow-Based Market Coupling Model and the Bidding Zone Configuration'. *SSRN Electronic Journal*. DOI: 10.2139/ssrn.3272190.

Bø, Andreas Hovde et al. (2020). 'The Impact of Flow-Based Market Coupling on the Nordic Region'. *2020 17th International Conference on the European Energy Market (EEM)*, pp. 1–6. DOI: 10.1109/EEM49802.2020.9221952.

Bolkesjø, Jon Rokne and Rønneseth, Maren Elise (2018). 'The Nordic flow-based market coupling - Utility value of adapted hydropower production'. MA thesis. Norwegian University of Life Sciences.

Brose, Eirik Braaten and Haugsbø, Andreas Sandal (2019). 'Flow-Based Market Coupling in the Nordic Power Market'. MA thesis. Norwegian School of Economics.

Chen, Yi-kuang et al. (2021). 'Long-Term Trends of Nordic Power Market: A Review'. *WIREs Energy and Environment* 10. DOI: 10.1002/wene.413.

Coffrin, Carleton et al. (June 2018). 'PowerModels.jl: An Open-Source Framework for Exploring Power Flow Formulations'. *2018 Power Systems Computation Conference (PSCC)*, pp. 1–8. DOI: 10.23919/PSCC.2018.8442948.

Commission Regulation (EU) 2015/1222, Establishing a Guideline on Capacity Allocation & Congestion Management (2015). https://eur-lex.europa.eu. *Official Journal of the European Union*.

Corona, Luis, Mochon, Asuncion and Saez, Yago (2022). 'Electricity Market Integration and Impact of Renewable Energy Sources in the Central Western Europe Region: Evolution since the Implementation of the Flow-Based Market Coupling Mechanism'. *Energy Reports* 8, pp. 1768–1788. DOI: 10.1016/j.egyr.2021.12.077.

Cui, Hui et al. (2021). 'A Review on Nord Pool Electricity Market: From ATC to Flow-based Clearing'. *2021 IEEE Sustainable Power and Energy Conference (iSPEC)*, pp. 1949–1954. DOI: 10.1109/iSPEC53008.2021.9735557.

Diniz, Andre Luiz and Souza, Thiago Mota (2014). 'Short-Term Hydrothermal Dispatch With River-Level and Routing Constraints'. *IEEE Transactions on Power Systems* 29, pp. 2427–2435. DOI: 10.1109/TPWRS.2014.2300755.

Eicke, Anselm and Schittekatte, Tim (2022). 'Fighting the wrong battle? A critical assessment of arguments against nodal electricity prices in the European debate'. *Energy Policy* 170. DOI: https://doi.org/10.1016/j.enpol.2022.113220.

Energinet et al. (2014). *Methodology and Concepts for the Nordic Flow Based Market Coupling*. https://www.fingrid.fi/flow-based. Accessed: 2023-01-21.

Euphemia Public Description (2020). https://www.nordpoolgroup.com/euphemia. Accessed: 2023-01-27.

Farahmand, Hossein (2021). Congestion Management. *TET4185, Power Markets, Resources and Environment*. https://ntnu.blackboard.com. Accessed: 2023-02-14.

Felten, Björn, Osinski, Paul and Weber, Christoph (2021). 'The Flow-Based Market Coupling Domain - Why We Can't Get It Right'. *Utilities Policy* 70. DOI: 10.1016/j.jup.2020.101136.

Finck, Rafael (2021). 'Impact of Flow Based Market Coupling on the European Electricity Markets'. *Sustainability Management Forum* 29, pp. 173–186. DOI: 10.1007/s00550-021-00520-w.

Flatabo, N. et al. (2003). 'Experience with the Nord Pool Design and Implementation'. *IEEE Transactions on Power Systems* 18, pp. 541–547. DOI: 10.1109/TPWRS.2003.810694.

Frank, Stephen and Rebennack, Steffen (2016). 'An introduction to optimal power flow: Theory, formulation, and examples '. *IIE Transactions* 48, pp. 1172–1197. DOI: 10.1080/0740817X.2016.1189626.

Haugen, Mari and Helseth, Arild (2021). *Primod – A Fundamental Short-Term Model for Power System Analyses and Multimarket Price Forecasting*. 2021:00376. Sintef Energy Research.

Haugen, Mari and Schäffer, Linn Emelie (2020). *Multimarket Modelling - Application of Different Models to HydroCen Low Emission Scenario*. HydroCen Report 16. Norwegian Research Centre for Hydropower Technology.

Helseth, Arild et al. (2018). 'Multi-Market Price Forecasting in Hydro-Thermal Power Systems'. *2018 15th International Conference on the European Energy Market (EEM)*, pp. 1–5. DOI: 10.1109/EEM.2018.8469932.

Hirvonen, Ritva (2022). *Overview of Assumptions and Parameters for the Beginning of External Parallel Run*. https://nordic-rcc.net/wp-content. Accessed: 2023-02-12.

Jegleim, Birgit (2015). 'Flow Based Market Coupling'. MA thesis. Norwegian University of Science and Technology.

Kristiansen, Tarjei (2019). 'The Flow Based Market Coupling Arrangement in Europe: Implications for Traders'. *Energy Strategy Reviews* 27. DOI: 10.1016/j.esr.2019.100444.

Lyngstad, Tølløv (2022). 'Flow-based Market Coupling in the Nordics'. [Unpublished paper], Norwegian University of Science and Technology.

Makrygiorgou, Despoina I. et al. (2020). 'Cross-Border Trading via Market Coupling in South East Europe Region'. *2020 17th International Conference on the European Energy Market (EEM)*, pp. 1–6. DOI: 10.1109/EEM49802.2020.9221995.

Mo, Birger and Helseth, Arild (2012). *Sammenligning av flyt- og ATC-basert markedsklarering*. Tech. rep. Sintef Energy Research.

Nordeng, Ragnhild Aker (2016). 'Flow based market clearing: estimation of net positions'. MA thesis. Norwegian University of Science and Technology.

Nordpoolgroup (2020). *Intraday market*. https://www.nordpoolgroup.com/Intraday-market. Accessed: 2023-01-29.

NVE-Atlas (2023). https://www.atlas.nve.no. Accessed: 2023-04-02.

Olje- og energidepartementet (2022). *The Power Market*. https://energifaktanorge.no. Accessed: 2023-01-24.

OpenJS (2016a). *deck.gl: WebGL2 powered geospatial visualization*. https://deck.gl/. Accessed: 2023-01-22.

— (2016b). *pydeck: High-scale spatial rendering in Python*. https://deck.gl/pydeck. Accessed: 2023-01-22.

Optimization with Pypower (2023). https://www.pandapower/opf. Accessed: 2023-04-22.

Ovaere, Marten et al. (2022). 'The Effect of Flow-Based Market Coupling on Cross-Border Exchange Volumes and Price Convergence in Central-Western European Electricity Markets'. *SSRN*. DOI: 10.2139/ssrn.4059778.

Regulation (EU) 2019/943, on the internal market for electricity (2019). https://eur-lex.europa.eu. *Official Journal of the European Union*.

Sarfati, Mahir, Hesamzadeh, Mohammad and Holmberg, Pär (2019). 'Production efficiency of nodal and zonal pricing in imperfectly competitive electricity markets'. *Energy Strategy Reviews*. DOI: https://doi.org/10.1016/j.esr.2019.02.004.

Schavemaker, Pieter H. and Beune, René J.L. (2013). 'Flow-Based Market Coupling and Bidding Zone Delimitation: Key Ingredients for an Efficient Capacity Allocation in a Zonal System'. *2013 10th International Conference on the European Energy Market (EEM)*, pp. 1–6. DOI: 10.1109/EEM.2013.6607366.

Sutter, Hando (2014). *Nord Pool Spot– Leading the Power Markets Integration*.

Svarstad, Vegard Bremerthun (2016). 'Flow based market clearing - GSK strategies'. MA thesis. Norwegian University of Science and Technology.

Thurner, L. et al. (Nov. 2018). 'pandapower — An Open-Source Python Tool for Convenient Modeling, Analysis, and Optimization of Electric Power Systems'. *IEEE Transactions on Power Systems* 33.6, pp. 6510–6521. DOI: 10.1109/TPWRS.2018.2829021.

Van den Bergh, Kenneth, Boury, Jonas and Delarue, Erik (2016). 'The Flow-Based Market Coupling in Central Western Europe: Concepts and Definitions'. *The Electricity Journal*. DOI: 10.1016/j.tej.2015.12.004.

Voswinkel, Simon et al. (2019). 'Flow-Based Market Coupling: What Drives Welfare in Europe's Electricity Market Design?' *Utilities Policy*. DOI: http://dx.doi.org/10.2139/ssrn.3424708.

Weinhold, Richard (2021). *Evaluating Policy Implications on the Restrictiveness of Flow-based Market Coupling with High Shares of Intermittent Generation: A Case Study for Central Western Europe*. DOI: 10.48550/arXiv.2109.04940.

Weinhold, Richard and Mieth, Robert (2022). *Uncertainty-Aware Capacity Allocation in Flow-Based Market Coupling*. DOI: 10.48550/arXiv.2109.04968.

Appendix

A Complete model notation

Table A.1: Indices.

Index	Description	Index	Description
t	Day	k	Time step
a	Price area	ab	Connection
h	Hydropower module	g	Thermal generating unit
d	Price elastic demand node	c	Cut
w	Week	n	PQ-curve segment

Table A.2: Sets.

Set	Description
$\mathcal{T}$	Set of days in the study horizon
$\mathcal{K}$	Set of time steps per day
$\mathcal{A}$	Set of price areas
$\mathcal{H}$	Set of hydropower modules
$\mathcal{H}_h^D$	Set of hydropower modules with discharge to module h
$\mathcal{H}_h^S$	Set of hydropower modules with bypass to module h
$\mathcal{H}_h^S$	Set of hydropower modules with spillage to module h
$\mathcal{G}$	Set of thermal generating units
$\mathcal{D}$	Set of price-elastic demands
$\mathcal{D}_a$	Set of price-elastic demands in area a, $\mathcal{D}_a \subset \mathcal{D}$
$\mathcal{L}$	Set of connections
$\mathcal{L}^S$	Set of connections within the synchronous area, $\mathcal{L}^S \subset \mathcal{L}$
$\mathcal{L}_a$	Set of connections to/from area a, $\mathcal{L}_a \subset \mathcal{L}$
$\mathcal{N}_h$	Set of segments on the PQ-curve of hydropower module h
$\mathcal{C}$	Set of cuts
$\mathcal{P}_a^W$	Set of wind parks in area a
$\mathcal{W}$	Set of weeks for which water values are provided

Table A.3: System parameters.

Parameter	**Description**
D_{akt}	Price inelastic demand in area a, step k, day t [MW]
P^{W}_{akt}	Wind production in area a, step k, day t [MW]
C^{D}_{dk}	Cost of price elastic demand d in step k, day t [10^3 €/MWh]
C^{E}_{a}	Cost of curtailment in area a [10^3 €]
RAM_{abkt}	Remaining available margin at connection ab [MW]
ATC_{ab}	Available transfer capacity at connection ab [MW]
$PTDF^{a'}_{abkt}$	PTDF on connection ab from area a'
T_t	Numerical value of day t, T_t = [1, 2, ..., 7]
W	The week for which the the problem is solved

Table A.4: Hydropower parameters.

Parameter	**Description**
B_{wc}	Constant value in cost function for week w, cut c [10^3 €]
Π_{hwc}	cut *c*oefficient for module h, week w, cut c [10^3 €/Mm^3]
C^{B*}, C^{S*}	Bypass and spillage spillage penalties [10^3 €/m^3/s]
C^B, C^S, C^D	Cost of bypass, spillage and discharge [10^3 €/m^3/s]
C^S_{hkt}	Start-up cost of hydro module h, step k, day t [10^3 €/MW]
I^R_{hkt}	Regulated inflow to module h, step k, day t [Mm^3]
I^U_{hkt}	Unegulated inflow to module h, step k, day t [Mm^3]
$\underline{R}_h$, $\bar{R}_h$	Min and max reservoir level of module h [Mm^3]
u_{h01}	Initial unit commitment status for module h [binary]
r_{h01}	Initial reservoir level for module h [binary]
$\underline{Q}^D_h$, $\bar{Q}^D_h$	Min and max discharge of module h [m^3/s]
$\underline{Q}^B_h$, $\bar{Q}^B_h$	Min and max bypass of module h [m^3/s]
$\underline{Q}^U_h$, $\bar{Q}^U_h$	Min and max capacity of tunnel to and from module h [m^3/s]
$\underline{P}_h$, $\bar{P}_h$	Min and max production capacity of module h [Mm^3]
$\bar{Q}^P_h$	Max pumping capacity of module h [Mm^3]
η^P_h	Pumping efficiency of module h
$\bar{Q}^D_{nhkt}$	Max discharge per PQ-segment n of module h, step k, day t [Mm^3]
$\underline{Q}^{D*}_h$	Min discharge corresponding to min production at h [m^3/s]
Γ	Conversion factor between water flow and volume
η_{nh}	Generation efficiency per PQ-curve segment n for module h
H_h	Relative head, referred to initial reservoir level, of module h [m]

Table A.5: Thermal power parameters.

Parameter	**Description**
C^G_{gkt}	Marginal cost of thermal unit g, step k, day t [10^3 €/MWh]
C^S_g	Start-up cost of thermal unit g [10^3 €]
$\underline{P}_{gkt}$, $\bar{P}_{gkt}$	Min and max production capacity of unit g, step k, day t [m^3/s]
u_{g01}	Initial commitment status of thermal unit g [binary]
T^U_g	Minimum uptime hours of thermal unit g [h]
T^D_g	Minimum downtime hours of thermal unit g [h]
T^{U0}_g	Hours thermal unit g has been up prior to step $k = 1$ [h]
T^{D0}_g	Hours thermal unit g has been down prior to step $k = 1$ [h]
T^{Ui}_g	Initial uptime required unit g, $min\{u_{g0}(T^U_g - T^{U0}_g), \lvert\mathcal{K}\rvert\}$ [h]
T^{Di}_g	Initial downtime required unit g, $min\{(1 - u_{g0})(T^D_g - T^{D0}_g), \lvert\mathcal{K}\rvert\}$ [h]
$\Delta\underline{P}^G_g$, $\Delta\bar{P}^G_g$	Max ramp-down and ramp-up rate of thermal unit g [MW/h]
$\Delta\underline{P}^{G*}_g$, $\Delta\bar{P}^{G*}_g$	Ramping rates of unit g when shut down or started up [MW/h]

Table A.6: Variables.

Variable	Description
System	
y^D_{dkt}	Amount of price elastic demand d covered in step k, day t [MW]
d_{akt}	Dumped power at zero cost in area a, step k, day t [MW]
y^E_{akt}	Power curtailment in area a, step k, day t [MW]
f_{abkt}	Power flow on connection ab, step k, day t [MW]
np_{akt}	Net position in area a, step k, day t [MW]
Hydropower	
r_{hkt}	Reservoir level at module h, step k, day t [Mm^3]
q^R_{hkt}	Release from module h, step k, day t [m^3/s]
q^D_{hkt}	Discharge from module h, step k, day t [m^3/s]
q^D_{nhkt}	Discharge per PQ-segment at module h, step k, day t [m^3/s]
q^B_{hkt}	Bypass from module h, step k, day t [m^3/s]
q^S_{hkt}	Spillage from module h, step k, day t [m^3/s]
q^U_{hkt}	Tunneling from module h (to another reservoir), step k, day t [m^3/s]
q^P_{hkt}	Pumping from module h, step k, day t [m^3/s]
q^T_{hkt}	Tanking to module h, step k, day t [m^3/s]
q^{Bviol}_{hkt}	Bypass violation at module h, step k, day t [m^3/s]
q^{Dviol}_{hkt}	Discharge violation at module h, step k, day t [m^3/s]
p_{hkt}	Production at module h, step k, day t [MW]
u_{hkt}	Unit commitment status for module h, step k, day t [binary]
c^S_{hkt}	Start up cost paid for module h, step k, day t [binary]
α^W_w	Future cost of hydropower operation from week w [10^3 €]
α_t	Future cost of hydropower operation from day t [10^3 €]
Thermal power	
p_{gkt}	Power generation at thermal unit g, step k, day t [MW]
u_{gkt}	Unit commitment status for unit g, step k, day t [binary]
w_{gkt}	Start-up at unit g, step k, day t [binary]
z_{gkt}	Shut-down at unit g, step k, day t [binary]

B Complete model formulation

Objective function

$$\begin{aligned}\min z = \sum_{k\in\mathcal{K}}\Bigg(&\sum_{g\in\mathcal{G}}\big(C^G_{gkt}p_{gkt} + C^S_g w_{gkt}\big) - \sum_{d\in\mathcal{D}} C^D_{dk} y^D_{dkt} \\ &+ \sum_{a\in\mathcal{A}} C^E_a y^E_{akt} + \sum_{h\in\mathcal{H}}\big(C^{B^*} q^S_{hkt} + C^{S^*} q^S_{hkt} + C^S q^{Bviol}_{hkt} \\ &+ C^D q^{Dviol}_{hkt} + C^T q^T_{hkt} + c^S_{hkt}\big)\Bigg) + \alpha_t, \qquad t\in\mathcal{T}\end{aligned} \tag{B.1}$$

Hydropower constraints

$$\begin{aligned}&r_{hkt} - r_{h,k-1,t} + \Gamma\big(q^R_{hkt} + q^S_{hkt} + q^P_{hkt} + q^U_{hkt} - q^T_{hkt}\big) \\ -\Gamma\Big(&\sum_{h'\in\mathcal{H}^D_h} q^D_{h'kt} + \sum_{h'\in\mathcal{H}^S_h} q^S_{h'kt} + \sum_{h'\in\mathcal{H}^S_h} q^S_{h'kt} + \sum_{h'\in\mathcal{H}^P_h} q^P_{h'kt} + \sum_{h'\in\mathcal{H}^U_h} q^U_{h'kt}\Big) \\ &= I^R_{hkt}, \qquad h\in\mathcal{H},\ k\in\mathcal{K},\ t\in\mathcal{T}\end{aligned} \tag{B.2}$$

$$\alpha^W_w - \sum_{h\in\mathcal{H}}\big(\Pi_{hwc} r_{hkt} - \Gamma q^T_{hkt}\big) \geq B_{wc}, \qquad \begin{matrix} w\in[W, W-1], \\ t\in\mathcal{T},\ c\in\mathcal{C},\ k=|\mathcal{K}|\end{matrix} \tag{B.3}$$

$$\alpha_t = \frac{T_t}{|\mathcal{T}|}\alpha^W_w + (1-\frac{T_t}{|\mathcal{T}|})\alpha^W_{w-1}, \qquad w=W,\ t\in\mathcal{T} \tag{B.4}$$

$$\Gamma\big(q^S_{hkt} + q^D_{hkt} - q^R_{hkt}\big) = I^U_{hkt}, \qquad h\in\mathcal{H},\ k\in\mathcal{K},\ t\in\mathcal{T} \tag{B.5}$$

$$\underline{P}_h \leq p_{hkt} \leq \bar{P}_h, \qquad h\in\mathcal{H},\ k\in\mathcal{K},\ t\in\mathcal{T} \tag{B.6}$$

$$\underline{R}_h \leq r_{hkt} \leq \bar{R}_h, \qquad h\in\mathcal{H},\ k\in\mathcal{K},\ t\in\mathcal{T} \tag{B.7}$$

$$\underline{Q}^D_h \leq q^D_{hkt} + q^{Dviol}_{hkt} \leq \bar{Q}^D_h, \qquad h\in\mathcal{H},\ k\in\mathcal{K},\ t\in\mathcal{T} \tag{B.8}$$

$$\underline{Q}^S_h \leq q^S_{hkt} + q^{Bviol}_{hkt} \leq \bar{Q}^S_h, \qquad h\in\mathcal{H},\ k\in\mathcal{K},\ t\in\mathcal{T} \tag{B.9}$$

$$q^D_{hkt} = u_{hkt}\underline{Q}^{D*}_h + \sum_{n\in\mathcal{N}^h} q^D_{nhkt}, \qquad h\in\mathcal{H},\ k\in\mathcal{K},\ t\in\mathcal{T} \tag{B.10}$$

$$0 \leq q^D_{nhkt} \leq u_{hkt}\bar{Q}^D_{nhkt}, \qquad n\in\mathcal{N}^h,\ h\in\mathcal{H},\ k\in\mathcal{K},\ t\in\mathcal{T} \tag{B.11}$$

$$p_{hkt} = u_{hkt}\underline{P}_h + \sum_{n\in\mathcal{N}^h} H_h\eta_{nh} q^D_{nhkt}, \qquad h\in\mathcal{H},\ k\in\mathcal{K},\ t\in\mathcal{T} \tag{B.12}$$

$$c^S_{hkt} \geq C^S_h\big(u_{hkt} - u_{h,k-1,t}\big), \qquad h\in\mathcal{H},\ k\in\mathcal{K},\ t\in\mathcal{T} \tag{B.13}$$

Thermal constraints

$$u_{g,k-1,t} - u_{gkt} + w_{gkt} - z_{gkt} = 0, \qquad g \in \mathcal{G},\ k \in \mathcal{K},\ t \in \mathcal{T} \tag{B.14}$$

$$w_{gkt} + z_{gkt} \leq 1, \qquad g \in \mathcal{G},\ k \in \mathcal{K},\ t \in \mathcal{T} \tag{B.15}$$

$$u_{gkt}\underline{P}_{gkt} \leq p_{gkt} \leq u_{gkt}\bar{P}_{gkt}, \qquad g \in \mathcal{G},\ k \in \mathcal{K},\ t \in \mathcal{T} \tag{B.16}$$

$$\sum_{k \in T_g^{Ui}} \big(1 - u_{gkt}\big) = 0, \qquad g \in \mathcal{G},\ t \in \mathcal{T} \tag{B.17}$$

$$\sum_{k'=k}^{k+T_g^U-1} u_{gk't} \geq T_g^U w_{gkt}, \qquad g \in \mathcal{G},\ k \in \big[T_g^{Ui}+1, ..., |\mathcal{K}| - T_g^U + 1\big],\ t \in \mathcal{T} \tag{B.18}$$

$$\sum_{k'=k}^{|\mathcal{K}|} \big(u_{gk't} - w_{gk't}\big) \geq 0, \qquad g \in \mathcal{G},\ k \in \big[|\mathcal{K}| - T_g^U + 2, ..., |\mathcal{K}|\big],\ t \in \mathcal{T} \tag{B.19}$$

$$\sum_{k \in T_g^{Di}} u_{gkt} = 0, \qquad g \in \mathcal{G},\ t \in \mathcal{T} \tag{B.20}$$

$$\sum_{k'=k}^{k+T_g^D-1} \big(1 - u_{gk't}\big) \geq T_g^D z_{gk't}, \qquad g \in \mathcal{G},\ k \in \big[T_g^{Di}+1, ..., |\mathcal{K}| - T_g^D + 1\big],\ t \in \mathcal{T} \tag{B.21}$$

$$\sum_{k'=k}^{|\mathcal{K}|} \big(1 - u_{gk't} - w_{gk't}\big) \geq 0, \qquad g \in \mathcal{G},\ k \in \big[|\mathcal{K}| - T_g^D + 2, ..., |\mathcal{K}|\big],\ t \in \mathcal{T} \tag{B.22}$$

$$p_{gkt} - p_{g,k-1,t} \leq u_{g,k-1,t}\Delta\bar{P}_g^G + w_{gkt}\Delta\bar{P}_g^{G*}, \qquad g \in \mathcal{G},\ k \in \mathcal{K} \tag{B.23}$$

$$-\big(p_{gkt} - p_{g,k-1,t}\big) \leq u_{gkt}\Delta\underline{P}_g^G, \qquad g \in \mathcal{G},\ k \in \mathcal{K} \tag{B.24}$$

CNTC specific constraints

$$\begin{aligned}\sum_{h\in\mathcal{H}} p_{hkt} - \eta_h^P q_{hkt}^P + \sum_{g\in\mathcal{G}} p_{gkt} - \sum_{d\in\mathcal{D}_a} y_{dkt}^D + \sum_{(a,b)\in\mathcal{L}_a} \left(f_{bakt} - f_{abkt}\right) \\ +y_{akt}^E - d_{akt} = D_{akt} - P_{akt}^W, \qquad a\in\mathcal{A},\ k\in\mathcal{K},\ t\in\mathcal{T}\end{aligned} \tag{B.25}$$

$$0 \le f_{abkt} \le ATC_{ab}, \qquad (a,b)\in\mathcal{L},\ k\in\mathcal{K},\ t\in\mathcal{T} \tag{B.26}$$

FBMC specific constraints

$$\begin{aligned}\sum_{h\in\mathcal{H}} p_{hkt} - \eta_h^P q_{hkt}^P + \sum_{g\in\mathcal{G}} p_{gkt} - \sum_{d\in\mathcal{D}_a} y_{dkt}^D + \sum_{(a,b)\in\mathcal{L}_a} \left(f_{bakt} - f_{abkt}\right) \\ +y_{akt}^E - d_{akt} = D_{akt} - P_{akt}^W, \qquad a\in\mathcal{A}\backslash\left\{\mathcal{A}^S\right\},\ k\in\mathcal{K},\ t\in\mathcal{T}\end{aligned} \tag{B.27}$$

$$\begin{aligned}np_{akt} = \sum_{h\in\mathcal{H}} p_{hkt} - \eta_h^P q_{hkt}^P + \sum_{g\in\mathcal{G}} p_{gkt} - \sum_{d\in\mathcal{D}_a} y_{dkt}^D + \sum_{\substack{(a,b)\in\mathcal{L}_a \\ b\notin\mathcal{A}^S}} \left(f_{bakt} - f_{abkt}\right) \\ +y_{akt}^E - d_{akt} - D_{akt} + P_{akt}^W, \qquad a\in\mathcal{A}^S,\ k\in\mathcal{K},\ t\in\mathcal{T}\end{aligned} \tag{B.28}$$

$$\sum_{a\in\mathcal{A}^S} np_{akt} = 0, \qquad k\in\mathcal{K},\ t\in\mathcal{T} \tag{B.29}$$

$$f_{abkt} = \sum_{a'\in\mathcal{A}^S} PTDF_{abkt}^{a'} \cdot np_{a'kt}, \qquad (a,b)\in\mathcal{L}^S,\ k\in\mathcal{K},\ t\in\mathcal{T} \tag{B.30}$$

$$0 \le f_{abkt} \le RAM_{abkt}, \qquad (a,b)\in\mathcal{L}^S,\ k\in\mathcal{K},\ t\in\mathcal{T} \tag{B.31}$$

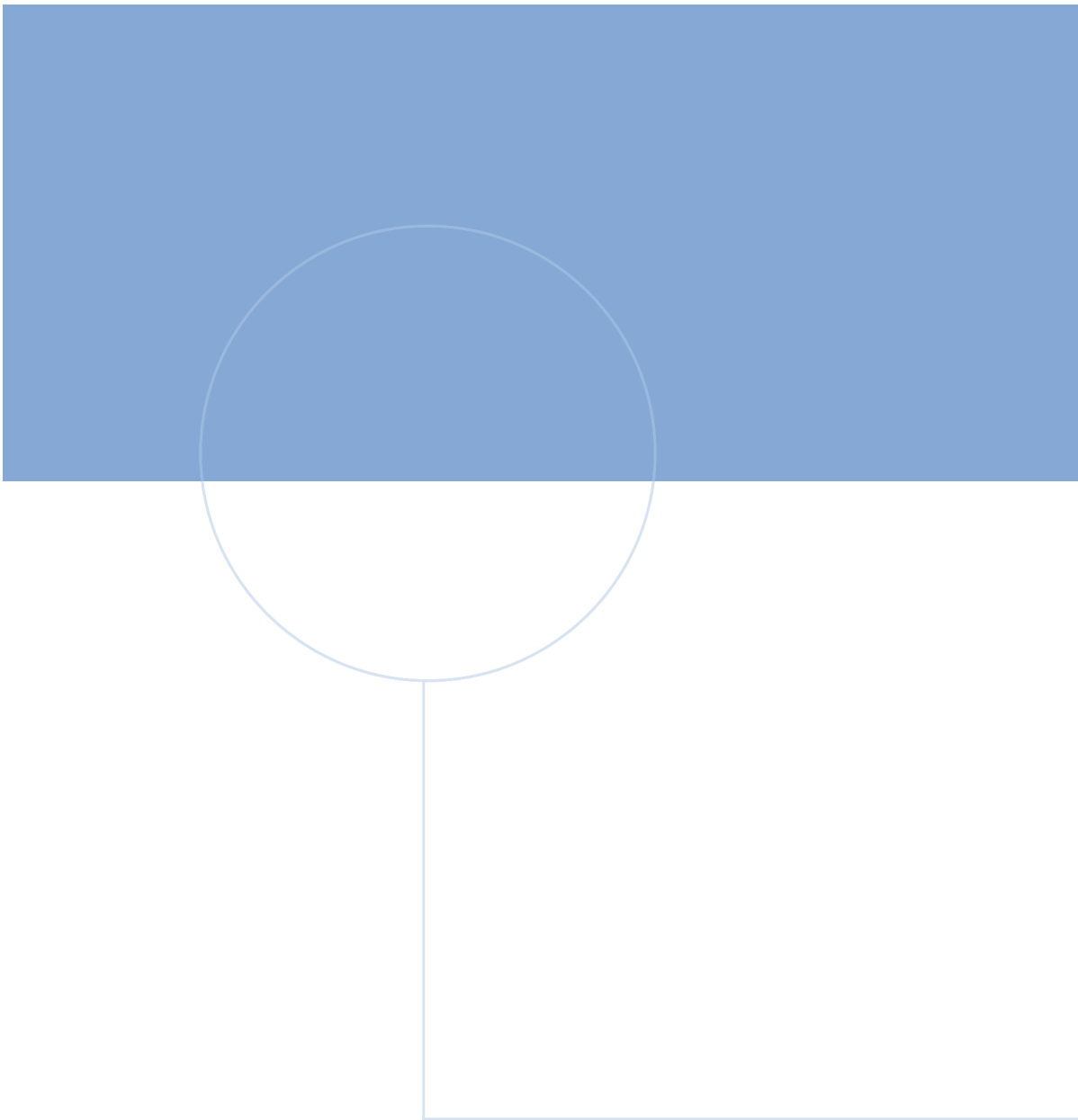

NTNU

Norwegian University of
Science and Technology